network

MDPI

Article

Direct-to-Cell NTN Systems in Terrestrial 5G Bands: Network-Level Sensitivity Analysis and PFD/EPFD Limits for Coexistence

Alexander Pastukh [1,*], Olga Mironova [1] and Valery Tikhvinskiy [2]

[1] The M.I. Krivosheev National Research Centre for Telecommunication (NRCT), 105064 Moscow, Russia; mironovaol@nic-t.ru
[2] National Research University Higher School of Economics (HSE University), 101000 Moscow, Russia; vtniir@mail.ru
* Correspondence: a.pastukh87@gmail.com

Abstract

Direct-to-cell (D2C) non-terrestrial networks (NTNs) based on 5G technology are emerging as a key complement to terrestrial cellular networks, extending connectivity to underserved and remote areas while enabling integration with existing mobile ecosystems. As these systems begin operating in frequency bands already used by terrestrial International Mobile Telecommunications (IMT) networks, coexistence becomes critical. This paper presents a victim-centric methodology for evaluating D2C interference into terrestrial 5G networks in the 694/698 MHz-2.7 GHz regulatory study range. Seven downlink carrier cases and four uplink carrier cases between 734 and 2620 MHz are evaluated. For a prescribed external interference-to-noise ratio, the external contribution is referenced to receiver thermal noise, while terrestrial intra-network interference remains part of the baseline and interfered signal-to-interference-plus-noise ratio (SINR). The resulting throughput loss is translated into candidate power-flux-density (PFD) and equivalent-power-flux-density (EPFD) protection levels. A reference non-geostationary-satellite-orbit (NGSO) system is used only to motivate the assumed receiver-exposure fractions; the numerical network results are therefore conditional on those exposure assumptions. The same external interference level produces approximately three times greater network throughput loss at base stations than at user equipment, so direction-specific protection levels are required. For downlink protection, the tested 3 dB noise-rise case gives candidate PFD levels from −109.23 to −98.17 dB(W/(m^2·MHz)); for opposite-direction cross-border uplink protection, I/N = −6 dB gives candidate EPFD levels from −138.23 to −130.18 dB(W/(m^2·MHz)) for non-AAS base stations. The approximately 11 dB offset for AAS cases results from the maximum-gain normalization used in EPFD and should not be interpreted as evidence of greater satellite exposure. These values are tested candidate levels rather than estimates of an exact 5% crossing point.

Keywords: direct-to-cell (D2C); NTN; spectrum compatibility; aggregate interference; 694/698 MHz-2.7 GHz; WRC-27

Check for updates

Academic Editor: Patrick Seeling

Received: 3 August 2026
Revised: 2 September 2026
Accepted: 4 September 2026
Published: 7 September 2026

Copyright: © 2026 by the authors. Licensee MDPI, Basel, Switzerland. This article is an open access article distributed under the terms and conditions of the Creative Commons Attribution (CC BY) license.

1. Introduction

Direct-to-cell (D2C) non-terrestrial networks are emerging as a practical extension of terrestrial mobile networks, providing service continuity in remote, underserved, and disaster-affected areas. Two distinct spectrum approaches must, however, be differentiated.

The NTN bands standardized by 3GPP to date, including bands n255 and n256 introduced for NR-NTN in Release 17, are frequency bands allocated to the mobile-satellite service (MSS). They are not the frequency bands deployed for the terrestrial component of IMT, and terrestrial LTE/5G networks do not operate co-channel with those standardized MSS-band NTN assignments [1–3].

The case considered in this paper is fundamentally different. WRC-27 agenda item 1.13, established through Resolution 253 (WRC-23), studies possible new MSS allocations between 694/698 MHz and 2.7 GHz in frequency ranges identified for terrestrial IMT and already used by operational LTE and 5G networks [4]. The objective is direct connectivity between space stations and conventional IMT user equipment, allowing existing, unmodified smartphones to receive satellite service without a dedicated satellite terminal. This approach therefore reuses terrestrial cellular spectrum rather than placing NTN only in separate MSS bands.

For consistency, this paper uses D2C to mean direct-to-cell satellite connectivity. ITU materials for WRC-27 agenda item 1.13 describe the same sharing scenario as direct connectivity between mobile-satellite service space stations and IMT user equipment, abbreviated here as DC-MSS-IMT. The term DC-MSS-IMT is retained only when referring specifically to that ITU nomenclature; D2C is used elsewhere.

This terrestrial frequency reuse creates the central coexistence problem addressed here. A satellite beam can illuminate territories of several countries at the same time, whereas national LTE/5G deployments may implement different IMT frequency arrangements or transmission directions. A satellite downlink transmitted on a terrestrial downlink frequency can interfere with IMT user equipment. More critically for cross-border coordination, the same frequency may be used for terrestrial downlink in one country and terrestrial uplink in a neighboring country, causing the satellite downlink to interfere with IMT base-station receivers. Protection criteria are therefore required for both user equipment and base stations and must reflect network-level performance and aggregate interference. The relevant technical framework is provided by the International Telecommunication Union Radiocommunication Sector (ITU-R), including Recommendation ITU-R M.2101, Report ITU-R M.2292, and Recommendation ITU-R M.1036 [5–7].

Related Work and Research Gap

The 3GPP studies supporting NR-NTN standardization established radio-frequency and coexistence requirements for satellite access in MSS bands, particularly n255 and n256, and examined compatibility with systems in adjacent bands [1–3]. This work demonstrated that NR waveforms and cellular-type user equipment can support satellite access. It did not, however, define co-channel protection limits for satellite transmissions reusing the frequency bands of operational terrestrial LTE/5G networks under the different national frequency arrangements considered by WRC-27 agenda item 1.13.

Broader architectural studies have identified propagation delay, Doppler shift, and PHY/MAC adaptation as central challenges in integrating satellite systems with terrestrial 5G networks [8].

Recent research has examined several complementary parts of the coexistence problem. Interference analyses have been reported for direct-to-cell operation in the n25 band and for NTN deployments in the L- and S-bands [9,10]. Coordinated dynamic spectrum-sharing methods have also been proposed to balance terrestrial-network protection and NTN resource availability [11]. In addition, controlled laboratory measurements of co-channel LEO-like downlink interference into terrestrial 5G receivers have shown that a 1 dB receiver desensitization occurs near an interference-to-noise ratio of −6 dB under the

tested conditions [12]. These contributions provide important link-level, band-specific, and resource-management results.

Earlier cognitive-satellite studies similarly formulated carrier, bandwidth, and transmit-power allocation under interference constraints intended to protect incumbent terrestrial networks [13].

Recent systems research has also examined multi-tenant LEO architectures capable of providing direct 4G/5G connectivity to conventional mobile phones and IoT devices [14].

A remaining need is therefore a consistent system-level assessment of the specific WRC-27 agenda item 1.13 scenario: satellite downlinks providing service to conventional IMT smartphones while reusing frequency bands already occupied by terrestrial LTE/5G. Such an assessment should connect satellite-generated interference to the throughput degradation of operational terrestrial networks across the 694/698 MHz to 2.7 GHz range. It must also address both same-direction protection of user equipment and opposite-direction protection of base stations, including cross-border cases in which neighboring countries use different frequency arrangements, and translate the resulting degradation into regulatory limits applicable to satellite emissions.

The contribution of this paper is a network-level sensitivity analysis that quantifies how a prescribed receiver degradation produces throughput degradation in an operational terrestrial 5G network, together with the conversion of that relationship into the required PFD and EPFD limits. Four specific outcomes follow.

First, the study provides a quantified mapping between externally applied receiver interference and network throughput loss for seven downlink carrier cases (734, 852, 925, 1805, 1900, 2110, and 2620 MHz) and four uplink carrier cases (734, 852, 1900, and 2620 MHz). Earlier work on direct-to-cell coexistence has addressed individual bands, link-level receiver desensitization or resource-coordination mechanisms; a common multi-band, multi-cell mapping of this kind has not been reported for this scenario.

Second, the results identify a marked asymmetry between the two link directions: the same prescribed noise rise produces an uplink throughput loss approximately three times the downlink loss. This is the principal empirical outcome of the study and shows that uplink protection requires more stringent, direction-specific limits.

Third, the study addresses the opposite-direction cross-border case in which a satellite downlink overlaps the terrestrial uplink of a neighboring country using a different frequency arrangement or duplexing scheme. This case arises specifically from the reuse of terrestrial IMT spectrum by D2C systems. The corresponding base-station limits are expressed as EPFD so that the directional receive gain of the victim receiver is accounted for. The approximately 11 dB offset between the AAS and non-AAS values is produced by the different maximum-gain normalizations in the EPFD conversion; it does not by itself indicate greater satellite exposure of AAS sites.

Fourth, because the degradation is prescribed at the victim receiver rather than generated by a specific interfering system, the resulting PFD and EPFD values are independent of NGSO architecture and can serve as a common compliance interface. The division of responsibility between a victim-side limit and a system-side compliance demonstration follows established practice for flux-density limits in the Radio Regulations; what is new here is that the limit is derived from an explicit, quantified network-performance criterion rather than from a receiver-level criterion alone.

The remainder of the paper is organized as follows. Section 2 defines the terrestrial IMT deployment and antenna parameters. Section 3 presents the system-level throughput-loss methodology and the conversion from receiver noise rise to PFD or EPFD. Sections 4 and 5 present the protection results for IMT user equipment and base stations, respectively.

Section 6 discusses the engineering and regulatory implications, and Section 7 summarizes the main conclusions.

2. Characteristics of IMT Systems in the 694/698-2690 MHz Frequency Range

The analysis uses the IMT deployment parameters presented in Tables 1 and 2, which are derived from Report ITU-R M.2292 and Recommendation ITU-R M.2101. The typical antenna pattern of the non-active antenna system (non-AAS) base station is shown in Figure 1. The beamforming antenna characteristics of the active antenna system (AAS) base station are provided in Table 3, and the corresponding composite antenna pattern is shown in Figure 2. These tables are derived from the corresponding Recommendations and Report of ITU-R [5,6,15,16], particularly Tables 1 and 2 are from Report ITU-R M.2292 and Table 3 is from the WRC-19 cycle Chairman's Report of WP 5D.

Table 1. Deployment-related parameters for bands below 1 GHz according to Report ITU-R M.2292 [6].

Base Station Characteristics/Cell Structure	
Cell radius	>5 km (typical 8 km) for macro rural scenario 0.5–5 km (typical 2 km) for macro urban/suburban scenario
Antenna height	30 m
Sectorization	3 sectors
Downtilt	3 degrees
Antenna pattern	Recommendation ITU-R F.1336 (recommends 3.1) • k_a = 0.7 • k_p = 0.7 • k_h = 0.7 • k_v = 0.3 Horizontal 3 dB beamwidth: 65 degrees Vertical 3 dB beamwidth: determined from the horizontal beamwidth by equations in Recommendation ITU-R F.1336. Vertical beamwidths of actual antennas may also be used when available.
Antenna polarization	Linear/±45 degrees
Feeder loss	3 dB
Maximum base station output power	46 dBm in 10 MHz
Base station antenna gain	15 dBi
Base station EIRP/sector	58 dBm in 10 MHz
Average base station activity factor	50%
Average base station EIRP/sector taking into account activity factor	55 dBm in 10 MHz
User Terminal Characteristics	
Indoor user terminal usage	50% for macro rural scenario 70% for macro urban/suburban scenario
Average indoor user terminal penetration loss	15 dB for macro rural scenario 20 dB for macro urban/suburban scenario
Maximum user terminal transmitter output power	23 dBm
Average user terminal transmitter output power	2 dBm for macro rural scenario –9 dBm for macro urban/suburban scenario
Antenna gain for user terminals	–3 dBi
Body loss	4 dB

Table 2. Deployment-related parameters for bands between 1 and 3 GHz according to Report ITU-R M.2292 and Recommendation ITU-R F.1336 [6,15].

Base Station Characteristics/Cell Structure	
Cell radius/deployment density (for bands between 1 and 2 GHz)	>3 km (typical figure to be used in sharing studies 5 km)
Cell radius/deployment density (for bands between 2 and 3 GHz)	>2 km (typical figure to be used in sharing studies 4 km)
Antenna height	30 m
Sectorization	3 sectors
Downtilt	3 degrees
Antenna pattern	Recommendation ITU-R F.1336 (recommends 3.1) • k_a = 0.7 • k_p = 0.7 • k_h = 0.7 • k_v = 0.3 Horizontal 3 dB beamwidth: 65 degrees Vertical 3 dB beamwidth: determined from the horizontal beamwidth by equations in Recommendation ITU-R F.1336. Vertical beamwidths of actual antennas may also be used when available.
Antenna polarization	Linear/±45 degrees
Below rooftop base station antenna deployment	0%
Feeder loss	3 dB
Maximum base station output power (5/10/20 MHz)	43/46/46 dBm
Maximum base station antenna gain	18 dBi
Maximum base station output power/sector (EIRP)	58/61/61 dBm
Average base station activity	50%
Average base station power/sector taking into account activity factor	55/58/58 dBm
User Terminal Characteristics	
Indoor user terminal usage	50%
Indoor user terminal penetration loss	15 dB
Maximum user terminal output power	23 dBm
Average user terminal output power	2 dBm
Typical antenna gain for user terminals	–3 dBi
Body loss	4 dB

Table 3. Beamforming antenna characteristics for IMT in the 1710–4990 MHz frequency range according to Document/716 Annex 4.4 of Working Party 5D ITU-R Chairman's Report and Recommendation ITU-R M.2101 [5,16].

Base Station Antenna Characteristics	
Antenna pattern	Refer to the extended AAS model in ITU-R Rec. M.2101
Element gain (dBi) (Note 1)	6.4
Horizontal/vertical 3 dB beamwidth of a single element (degree)	90° for H; 65° for V
Horizontal/vertical front-to-back—ratio (dB)	30 for both H/V
Antenna polarization	Linear ±45°

Table 3. *Cont.*

Antenna array configuration (Row × Column) (Note 2)	4 × 8 elements
Horizontal/Vertical radiating element/sub-array spacing, *dh/dv*	0.5 of wavelength for H, 2.1 of wavelength for V
Number of element rows in sub-array, M_{sub}	3
Vertical radiating element spacing in sub-array, $d_{v,sub}$	0.7 of a wavelength for V
Pre-set sub-array downtilt, $\theta_{subtilt}$ (degrees)	3
Array Ohmic loss (dB) (Note 1)	2
Conducted power (before Ohmic loss) per antenna element/sub-array (dBm) (Note 5)	28
Base station horizontal coverage range (degrees)	±60
Base station vertical coverage range (degrees) (Notes 3, 4, 6)	90–100
Mechanical downtilt (degrees) (Note 4)	3
Maximum base station output power/sector (EIRP) (dBm)	72.28

Note 1: The element gain in row 1.2 includes the loss given in row 1.8 and is per polarization. This means that this parameter in row 1.8 is not needed for the calculation of the BS composite antenna gain and EIRP. Note 2: For the small/micro cell case, 8 × 8 means there are 8 vertical and 8 horizontal radiating elements. For the extended AAS model case, 4 × 8 means there are 4 vertical and 8 horizontal radiating sub-arrays. Note 3: The vertical coverage range is given in global coordinate system, i.e., 90° being at the horizon. Note 4: The vertical coverage range includes the mechanical downtilt. Note 5: The conducted power per element assumes 8 × 8 × 2 elements for the micro/small cell case, and 4 × 8 × 2 sub-arrays for the macro case (i.e., power per H/V-polarized element). Note 6: In sharing studies, the UEs that are below the base station vertical coverage range can be considered to be served by the "lower" bound of the electrical beam, i.e., the beam steered toward the max. coverage angle. A minimum BS-UE distance along the ground of 35 m should be used for urban/suburban and rural macro environments.

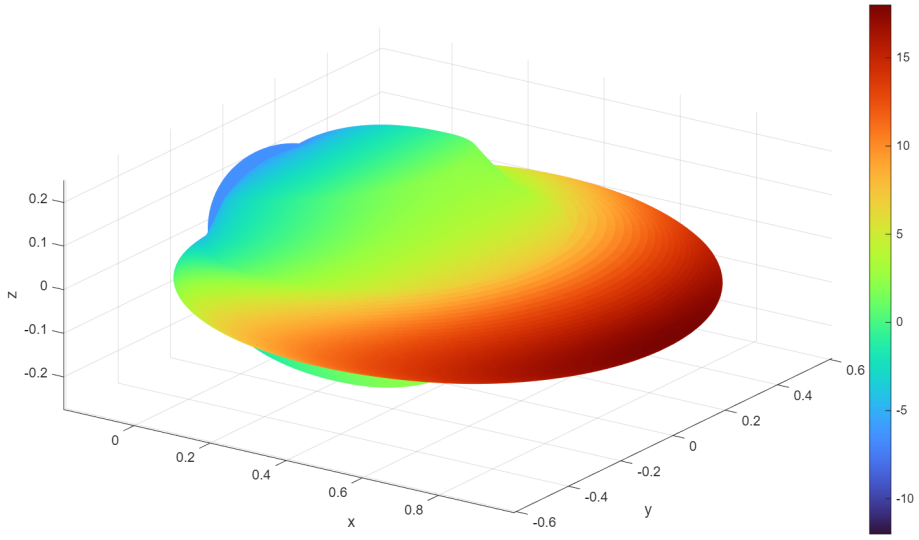


Figure 1. Typical three-dimensional antenna pattern of a non-AAS IMT base station.

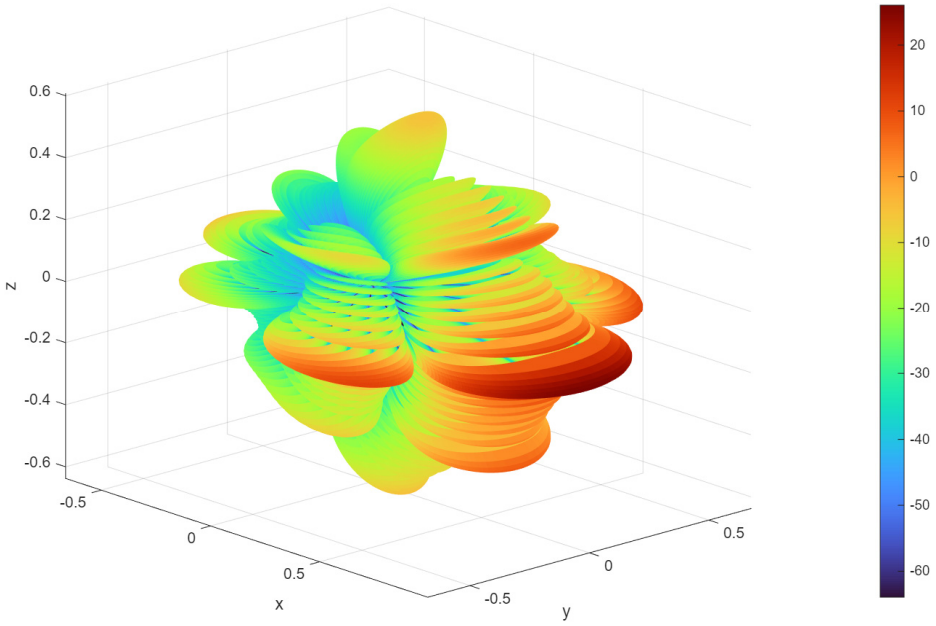


Figure 2. Typical composite antenna pattern of an AAS IMT base station in the 1880–1920 MHz and 2500–2690 MHz frequency bands.

3. Methodology for Throughput-Loss Assessment and PFD/EPFD Derivation

The methodology deliberately separates protection of the terrestrial victim network from the design of a particular interfering D2C system. The effect of D2C interference is evaluated by comparing a baseline terrestrial IMT simulation with paired cases in which a prescribed interference-induced noise rise is added at selected receivers. A specific satellite constellation, orbital geometry, propagation path, beam layout, and set of individual satellite signals are therefore not explicitly simulated in the throughput-sensitivity calculation.

This choice is intentional. D2C systems can differ substantially in orbital altitude and geometry, satellite and beam antenna patterns, the number and width of active beams, frequency-reuse arrangements, traffic loading, power control, duty cycle, and operational modes. A compatibility result obtained for one selected constellation would consequently apply only to that implementation and could not establish whether other NGSO designs protect terrestrial IMT receivers. The present approach instead determines the maximum receiver-side interference that the terrestrial network can tolerate under a defined throughput-loss criterion and expresses that interference as a PFD or EPFD protection limit.

The resulting limit provides a common regulatory interface between the victim and interfering systems, subject to the terrestrial deployment and exposure assumptions stated in this paper. Each proposed D2C system can use its own constellation geometry, beam configuration, frequency reuse, loading, and propagation assumptions to calculate the PFD or EPFD produced at the relevant IMT receiver and demonstrate that the applicable limit is not exceeded. This eliminates the need to repeat the terrestrial system-level throughput simulation for every NGSO architecture, while retaining the need for each operator to perform a system-specific emission and propagation assessment as part of its compliance demonstration. Each terrestrial-network configuration evaluated here comprises 5000 paired Monte Carlo snapshots. Every snapshot includes user generation and association, resource scheduling, desired-signal calculation, intra-network interference and receiver-noise calculation, application of the prescribed receiver noise rise, SINR-to-spectral-efficiency mapping, and aggregation of user throughput. The procedure is applied separately to the downlink and uplink.

3.1. Network Topology, User Association, and Scheduling

Step 1: For each Monte Carlo snapshot, construct a cluster of 19 tri-sector sites, corresponding to 57 cells. With K = 3 scheduled UEs per cell, drop 5K = 15 candidate UEs uniformly in each sector hexagon. The candidate locations and propagation realizations are regenerated for every snapshot.

Step 2: Calculate the path coupling loss from every candidate UE to every sector, including propagation loss, fading, and the applicable antenna gains, with a 70 dB minimum coupling loss. Each candidate is associated at random with one of the sectors whose coupling loss is within 3 dB of the minimum. If any sector receives fewer than K candidates, the candidate drop is repeated.

Step 3: Select K = 3 associated candidates at random in every cell, thereby enforcing exactly 171 simultaneously scheduled UEs in each snapshot. A 5 MHz channel with 15 kHz subcarrier spacing provides 25 resource blocks (RBs); each scheduled UE receives n = 8 RBs, so 24 RBs are used by the three equal scheduling chunks and one residual RB is unassigned. When beamforming is used, the serving base-station and UE beams are directed toward each other. The scheduler is round robin and does not use instantaneous channel quality.

The common simulation configuration is as follows: inter-site distance 6 km (sector-hexagon radius 2 km) for the carriers 1–3 GHz and 12 km (sector-hexagon radius 4 km) for the carriers below 1 GHz, minimum UE-BS distance 35 m, base-station power 46 dBm per sector, non-AAS pattern per Recommendation ITU-R F.1336 unless an AAS case is explicitly identified, UE maximum power 23 dBm, P0_PUSCH = −92.2 dBm/RB, fractional power-control factor α = 0.8, 5 MHz bandwidth, 15 kHz subcarrier spacing, 25 available RBs, and 8 RBs per scheduled UE. AAS cases use the array configuration reported in Table 3.

The value 171 denotes simultaneous scheduled links per snapshot, not the total registered subscriber population. A larger registered population, such as 5000 UEs, can be represented by drawing candidates and scheduling different subsets over successive snapshots. Modeling 5000 simultaneously active UEs in a 5 MHz channel would require a different traffic, resource-allocation, and load model. Computational cost grows approximately with the number of candidate UE-to-sector coupling calculations and with the number of scheduled co-channel links retained for interference evaluation.

3.2. Desired Signal, Intra-Network Interference, and Receiver Noise

The desired received power and the interference-plus-noise power are evaluated for every scheduled UE. In the downlink, the serving base station provides the desired signal and all non-serving base stations contribute intra-network interference. In the uplink, the desired signal is received from the scheduled UE in the serving cell and simultaneously scheduled UEs in the other cells contribute intra-network interference.

For AAS inter-cell interference, RB chunk k in every interfering sector is transmitted toward that sector's own scheduled UE k. The composite gain from the interfering sector toward the victim receiver is then evaluated at the corresponding off-axis direction. Thus, an interfering beam is not steered toward the victim UE; the victim generally sees a side-lobe or off-boresight gain of a beam serving another UE.

Step 4: Let P_{BS}^{Max} denote the maximum base-station transmit power, M = nK the number of RBs assigned across the K scheduled users, and P_{BS}^{UE} the power allocated to one scheduled UE over its n RBs:

$$P_{BS}^{UE} = P_{BS}^{Max} \frac{n}{M} \quad (1)$$

Step 5: For scheduled UE k in cell j, the desired received power is denoted by C(j,k) and the aggregate interference power by I(j,k).

For the downlink case, *C (j, k)* is the received power from the serving BS, i.e., the *j*-th BS.

$$C(j,\ k) = P_{BS}^{UE} \times pathCouplingLoss(UE_{j,k},\ BS_j) \quad (2)$$

For the uplink, $C(j,k)$ is the received power from $UE_{j,k}$, at the *j*-th BS:

$$C(j,\ k) = P_{PUSCH}(j,k) \times pathCouplingLoss(UE_{j,k},\ BS_j) \quad (3)$$

Step 6: *I (j, k)* is the interference power which consists of intra-system interference (from other cells in the same network) $I_{intra}(j,k)$, and receiver thermal noise N_t; external D2C interference is added separately in Step 7.

$$I(j,k) = I_{intra}(j,k) + N_t \quad (4)$$

$$I_{intra}(j,k) = \sum_{l=1,l\neq j}^{N_{cell}} P_{BS}^{UE} \times pathCouplingLoss(UE_{j,k}, BS_l) \quad (5)$$

The receiver thermal-noise power over the n-RB allocation bandwidth can be expressed as follows:

$$N_t = 10\text{ˆ}((10log_{10}(kT) + 10log_{10}(bandwithofnRBs) + NoiseFigure_{UE})/10) \quad (6)$$

For the uplink, the intra-network interference at base station j is as follows:

$$I_{intra}(j,k) = \sum_{l=1,l\neq j}^{N_{cell}} P_{PUSCH}(l,k) \times pathCouplingLoss(UE_{l,k}, BS_j) \quad (7)$$

UE power control is applied according to the following algorithm [17]:

$$P_{PUSH}(i) = \min(P_{CMAX},\ 10log_{10}(M_{PUSH}(i)) + P_{O_{PUSH}}(j) + \alpha(j)\cdot PL) \quad (8)$$

where the following applies:

P_{PUSCH}: transmit power of the terminal in dBm;
P_{CMAX}: maximum transmit power in dBm;
M_{PUSCH}: number of allocated RBs;
P_{0_PUSCH}: target power per RB in dBm;
a: balancing factor for UEs with bad channel and UEs with good channel;
PL: path loss in dB for the UE from its serving BS.

3.3. Statistical Emulation of Satellite Interference

Step 7: Represent D2C interference by an external interference-to-noise ratio $\rho = I_{ext}/N$ referenced exclusively to receiver thermal noise N. In the downlink assessment, the prescribed noise rise is applied to 50% of the UEs. The remaining 50% are assumed to be indoors and therefore not to receive appreciable satellite interference due to the wall loss of at least 15 dB. For the uplink, 70% of base stations are assumed to be exposed, whereas the remaining 30% are assumed to be oriented with their backlobes toward the areas served by D2C systems. These fractions are statistical exposure assumptions motivated by the reference-system analysis in Section 3.7 and do not form part of the definition of I/N.

For each exposed receiver, the baseline and interfered ratios are $SINR_0 = S/(I_{intra} + N)$ and $SINR_1 = S/(I_{intra} + N + I_{ext})$, respectively.

For a prescribed ρ in decibels, the external contribution used in the simulation is $I_{ext} = N\cdot 10\text{ˆ}(\rho/10)$. The terrestrial intra-network term I_{intra} is unchanged between the paired baseline and interfered calculations.

The external contribution is therefore not obtained by scaling the loaded quantity $I_{intra} + N$. The corresponding thermal-noise rise is $NR_N = 10log10[(N + I_{ext})/N] =$

10log10[1 + 10^(ρ/10)]. The evaluated ρ values −6, −5, −4, −3, and 0 dB correspond to NR_N values 0.97, 1.19, 1.46, 1.76, and 3.01 dB, displayed in the figures and tables as 1.00, 1.19, 1.46, 1.76, and 3.00 dB. I_{intra} affects SINR and throughput loss, but it is not included in the ITU-R I/N normalization.

$$I(j,k) = I_{intra}(j,k) + I_{external}(j,k) + N_t \quad (9)$$

3.4. SINR-to-Throughput Mapping

Step 8: Convert the SINR of every scheduled link to spectral efficiency using the following piecewise approximation of link adaptation. The Shannon bound is scaled by an implementation-loss factor and limited by the minimum and maximum SINR values supported by the assumed modulation and coding set [17]:

$$Spectral\ efficiency\ (SINR)\ [bps/Hz] = \begin{cases} 0 & for\ SINR \le SINR_{MIN} \\ \alpha_factor \cdot S(SINR) & for\ SINR_{MIN} < SINR < SINR_{Max} \\ \alpha_factor \cdot S(SINR_{Max}) & for\ SINR \ge SINR_{Max} \end{cases}$$

where the following applies:

$S(SINR)$: Shannon bound, $S(SINR) = \log_2(1 + SINR)$[bps/Hz];
α_factor: Attenuation factor, representing implementation losses;
$SINR_{Min}$: Minimum SINR of the code set [dB];
$SINR_{Max}$: Maximum SINR of the code set [dB].

The SINR thresholds listed in Table 4 are expressed in decibels and are converted to linear scale before application of the spectral-efficiency equation.

Table 4. Parameters describing baseline link-level performance for 5G NR.

Parameter	DL	UL	Notes
α_factor	0.6	0.4	Represents implementation losses
$SINR_{MIN}$ [dB]	–10	–10	Based on QPSK, 1/8 rate (DL) and 1/5 rate (UL)
$SINR_{Max}$ [dB]	30	22	Based on 256QAM 0.93(DL) and 64QAM 0.93 (UL)

The parameters $SINR_{MIN}$ and $SINR_{MAX}$ can be chosen to represent different modem implementations and link conditions.

For each snapshot, the throughput of a scheduled UE is obtained from its spectral efficiency and its allocated share of the 5 MHz channel bandwidth. Cell throughput is the sum over the scheduled UEs, and network throughput is the sum over the evaluated cells. For a baseline throughput T0 and an interfered throughput TI, the reported percentage loss is 100 × (T0 − TI)/T0. The throughput CDFs are formed from the corresponding Monte Carlo results.

3.5. Monte Carlo Scenarios and Receiver-Exposure Assumptions

The terrestrial IMT network is represented by the 19-site, 57-cell tri-sector cluster described above, with three scheduled UEs per cell and a 5 MHz channel bandwidth. Each configuration is evaluated over 5000 Monte Carlo snapshots, with UE locations randomly regenerated for successive snapshots. Terrestrial propagation is modeled using the 3GPP TR 38.901 Rural Macro (RMa) channel model with probabilistic line-of-sight conditions [18,19]. UE association is based on minimum path coupling loss with a 3 dB handover margin. The Rural Macro model is adopted deliberately to represent a bounding cross-border interference case. In this environment, satellite interference reaches terrestrial

receivers with little or no clutter attenuation, whereas in urban and suburban scenarios buildings shield both base stations and UEs, especially at low elevation angles; a greater share of UEs are also indoors and benefit from building-entry loss [18,19]. The rural scenario therefore produces a larger interference contribution at the victim receiver for a given incident flux density. Second, rural macro cells are substantially larger, so a greater proportion of users operate near the cell edge at a lower baseline $C/(N + I_{ext})$, where a given I_{ext}/N degradation removes a larger fraction of achievable spectral efficiency. Third, the near-border areas in which interference is likely to be greatest are often rural and sparsely populated, making rural deployments particularly susceptible. Applying the Rural Macro model at all evaluated frequencies therefore produces protection limits that remain valid for less exposed deployment types.

Network performance is first evaluated without external interference to establish the reference throughput. D2C interference is then introduced as a prescribed increase in the effective noise floor of the exposed receivers. The evaluated receiver noise-rise levels are 1.00, 1.19, 1.46, 1.76, and 3.00 dB, matching the cases reported in the throughput figures and tables.

Receiver exposure is represented statistically. For the downlink, 50% of UEs are assigned the prescribed noise rise and 50% are treated as indoor UEs with negligible received satellite interference due to building entry losses. For the uplink, 70% of base stations are assumed to be exposed, whereas the remaining 30% are assumed to be oriented with their backlobes toward the areas served by D2C systems.

This abstraction captures partial network exposure without requiring a satellite constellation or time-dependent geometry simulation. Figure 3 shows an example of terrestrial-network realization.

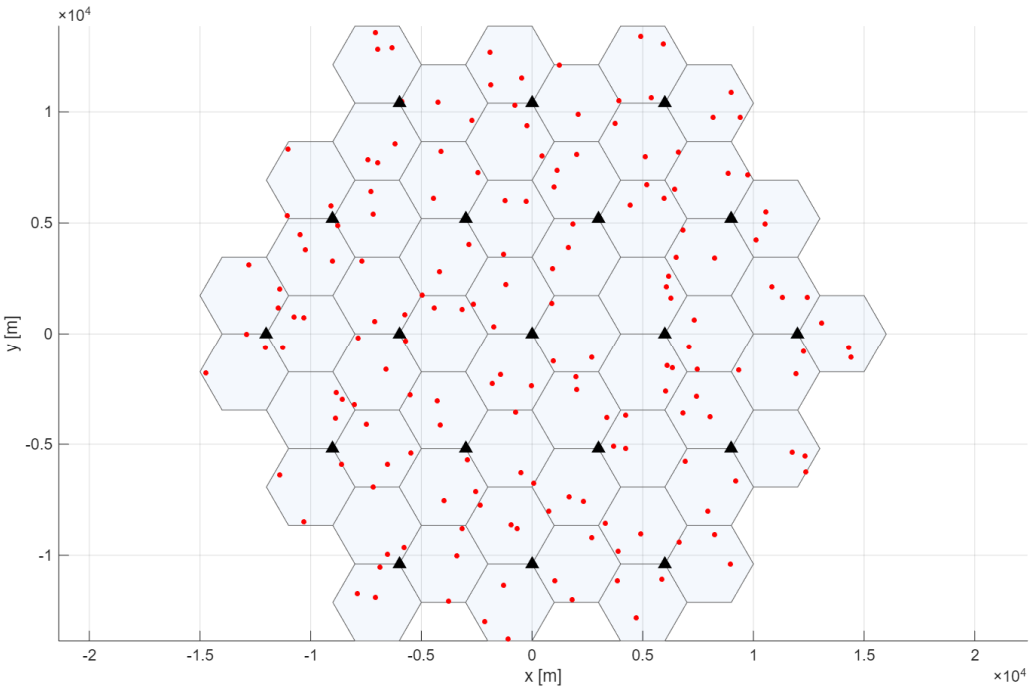


Figure 3. Example of tri-sector IMT network geometry showing base-station sites, sector coverage areas, and randomly distributed user equipment.

Results are retained at two spatial scopes. For each configuration, the reference cell is selected from sectors on the outer ring as the edge sector with the lowest mean downlink intra-network over Monte Carlo run. Figure 4 shows the selected reference sector for the illustrated 2110 MHz case. The reference-cell result therefore provides a deliberately

favorable edge-sensitive comparison, while the full-network metric averages the response over all 57 sectors.

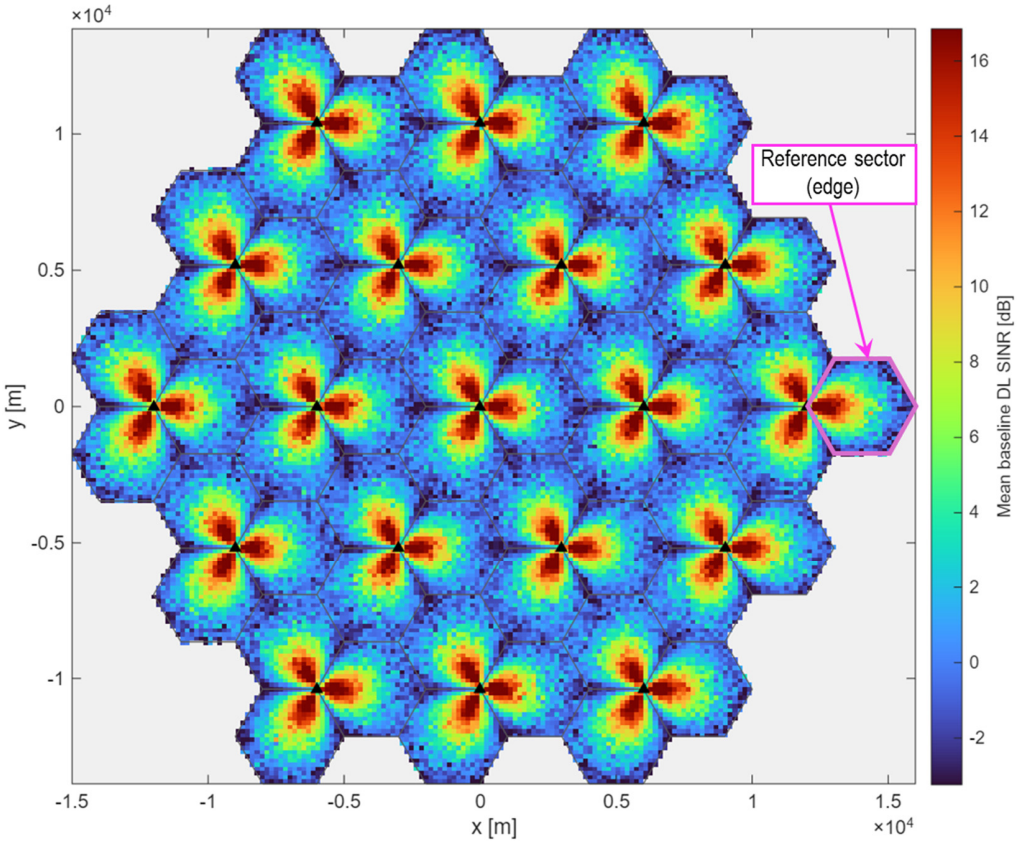


Figure 4. Mean baseline downlink SINR over the finite 19-site, 57-cell network at 2110 MHz. The outlined east-facing sector of the rightmost site is the reference cell. No wrap-around interference is used.

No wrap-around replication or periodic boundary condition is used: desired and interfering signals are calculated only for the 19 sites in the simulated cluster. Consequently, sectors near the cluster boundary have fewer in-cluster interferers than sectors in an infinite or periodically replicated deployment. The full-network average includes these edge sectors and may therefore be optimistic, while the selected reference sector represents an especially favorable boundary case. Both reporting scopes should be interpreted as conditional on this finite-cluster geometry rather than as wrap-around network results.

Before fixing the simulation length, Monte Carlo convergence was checked for the 2110 MHz downlink case with a 3 dB receiver noise rise and 1900 MHz UL with 1.19 dB noise rise. The baseline and interfered calculations are paired snapshot by snapshot using common random numbers: for pair i, both calculations reuse the same UE locations, line-of-sight and propagation/fading realizations, cell associations, exposure assignments, and scheduling decisions. The interfered member differs only by the prescribed external noise-rise term. UE locations and other random quantities are regenerated for the next pair. Pairing isolates the incremental D2C interference effect and substantially reduces the sampling uncertainty of throughput loss compared with independent baseline and interfered runs. The run length is N = 5000 snapshots and the stability-window length is W = 1000 snapshots, corresponding to n = 4000–5000 in Figures 5 and 6.

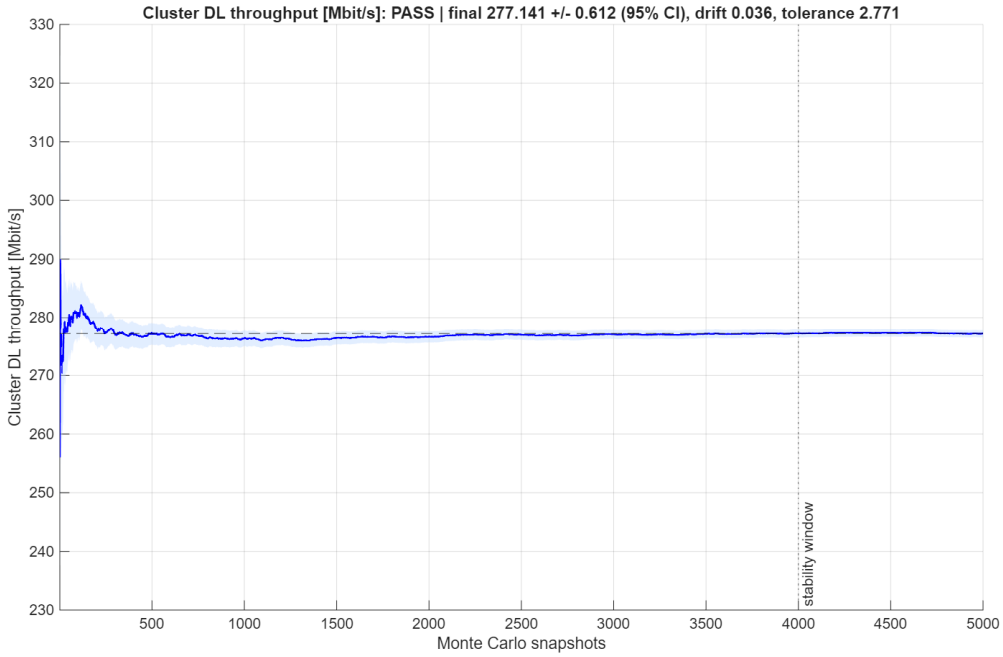


Figure 5. Monte Carlo convergence of aggregate downlink cluster throughput for the 2110 MHz, 3 dB receiver noise-rise case. The dashed vertical line marks the start of the 4000–5000-snapshot stability window; the shaded band denotes the 95% confidence interval.

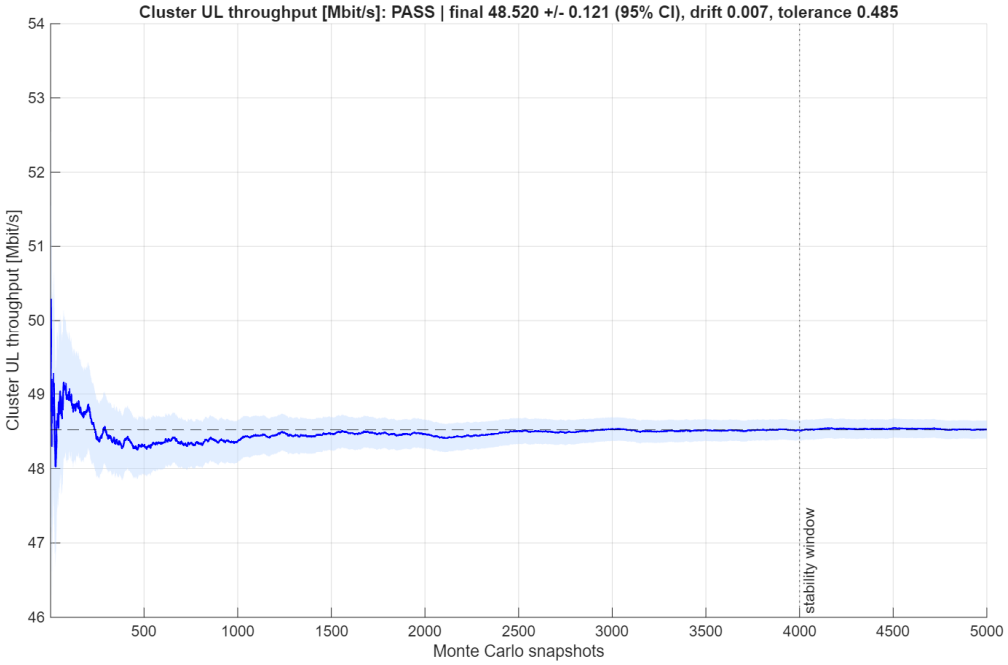


Figure 6. Monte Carlo convergence of aggregate uplink cluster throughput for the 1900 MHz, 1.19 dB receiver noise-rise case. The dashed vertical line marks the start of the 4000–5000-snapshot stability window; the shaded band denotes the 95% confidence interval.

Figures 7 and 8 indicate the terrestrial intra-network interference I_{intra} present in the paired baseline and interfered SINR calculations. In the downlink, the median lies between −102.4 dBm at 925 MHz and −95.8 dBm at 1805 MHz for non-AAS base stations, with a pronounced upper tail. In the uplink, the median lies between −120.2 and −116.5 dBm, and the upper tail is lighter because uplink power-control limits many strong contributions. Active antenna systems lower the uplink median by approximately 6 dB through off-axis

receive-gain effects. These distributions describe the operating regime of the terrestrial network; they are not used to redefine or rescale the external I_{ext}/N criterion.

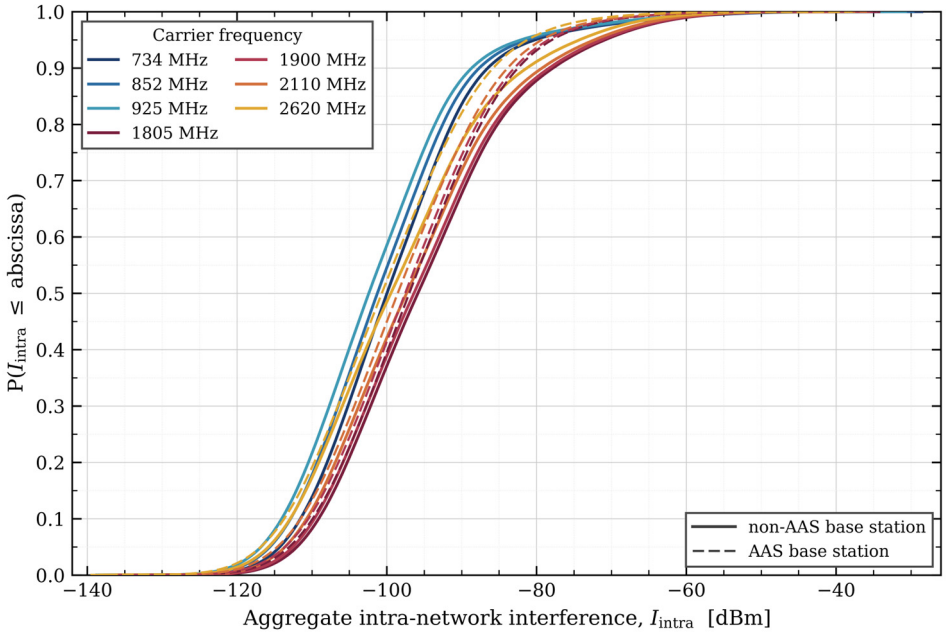


Figure 7. Cumulative distribution of the aggregate intra-network interference received by a scheduled user equipment in its resource-block allocation, downlink, for the evaluated carrier frequencies and base-station antenna configurations.

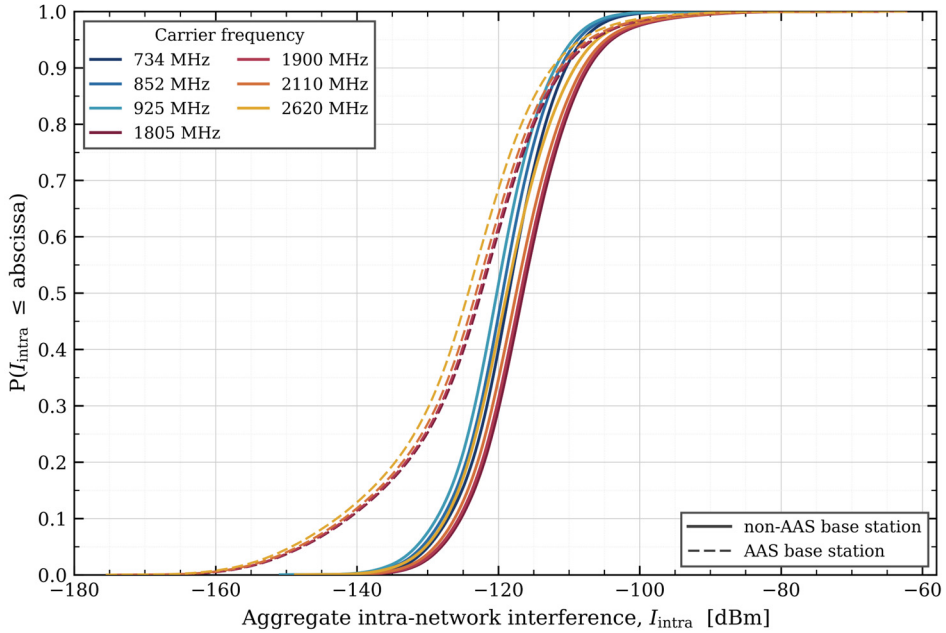


Figure 8. Cumulative distribution of the aggregate intra-network interference received by a base station in the resource-block allocation of a scheduled user, uplink, for the evaluated carrier frequencies and base-station antenna configurations.

Because I_{ext} is fixed relative to thermal noise, its marginal effect on SINR depends on the existing I_{ext}/N of each link. A more interference-limited downlink has a larger I_{intra} term in both $SINR_0$ and $SINR_1$ and is therefore less sensitive to the same I_{ext}/N than the more noise-limited uplink. This is the physical origin of the direction-dependent throughput response reported below.

3.6. Selection of Protection Criteria and Conversion from Receiver Noise Rise to PFD/EPFD

The external interference ratio and thermal-noise rise are related by $NR_N = 10\ log10[1 + 10\hat{}(I_{ext}/N/10)]$. Thus, $I_{ext}/N = -6$ dB gives $NR_N = 0.97$ dB and $I_{ext}/N = 0$ dB gives $NR_N = 3.01$ dB. Recommendation ITU-R M.2101 and Report ITU-R M.2292 identify $I/N = -6$ dB as a conventional receiver-protection criterion for IMT sharing studies [5,6]. In addition, this study adopts 5% full-network throughput loss values as a selected engineering screening ceiling. It is not presented as a normative ITU-R threshold or as a statistically estimated exact performance boundary.

For the downlink, the primary decision metric is the aggregate throughput loss of the full 57-cell network; the reference-cell result is supplementary. The 0 dB I_{ext}/N case (3.01 dB thermal-noise rise, displayed as 3 dB) is the highest evaluated grid point and gives network-wide loss is 3.39–4.95% in the seven evaluated bands. It is therefore retained as a tested candidate protection case under the stated exposure assumptions. Because no finder sweep above this grid point was performed, the result is not described as the maximum tolerable interference or as the exact 5% crossing.

For the uplink, $I_{ext}/N = -6$ dB (0.97 dB rise, displayed as 1 dB) gives a network-wide loss of 4.13–4.54%. The next evaluated point, $I_{ext}/N = -5$ dB (1.19 dB rise), gives 5.01–5.49%. The -6 dB point is therefore retained as the highest tested grid value below the screening ceiling in all four uplink cases and as a conservative candidate level, not an estimate of the exact crossing.

After evaluating throughput at each thermal-noise-referenced I_{ext}/N level over the 5 MHz simulation channel, the same external interference power is converted analytically to a power-flux-density level normalized to a 1 MHz reference bandwidth [20]. The throughput calculation and power-flux-density conversion therefore use the same N reference.

A receiver noise figure of 9 dB is used for the UE downlink calculation, and a receiver noise figure of 5 dB is used for the base-station uplink calculation. For UE protection, the conversion gives a PFD limit using the effective UE antenna gain. The corresponding base-station calculation is expressed as an EPFD limit so that the directional base-station antenna gain is incorporated. The receiver-noise relationship is as follows:

$$pfd = 10log_{10}(kT_0B) + \mathrm{NF} + 10log_{10}(10^{\frac{(N+I_{ext})/N}{10}} - 1) - G_r(\theta) + \mathrm{L} - 10log_{10}\left(\frac{\lambda^2}{4\pi}\right) \quad (10)$$

where the following applies:

k: Boltzmann's constant (1.380649×10^{-23} J/K);
T_0: receiver thermal noise in K;
B: reference bandwidth (1 MHz);
NF: receiver noise figure in dB;
$(N + I_{ext})/N$: thermal-noise rise corresponding to the applied external interference in dB;
$G_r(\theta)$: effective antenna gain in dBi of the receiver antenna in the direction of the interferer;
θ: the elevation angle;
L: Receiver antenna feeder loss for IMT BS and body loss for IMT UE.

The conversion is evaluated separately for every considered frequency because the wavelength-dependent effective aperture and the applicable receiver antenna characteristics differ by band. No satellite orbit, ephemeris, elevation track, or time-dependent link geometry enters the network simulation; satellite interference is parameterized by receiver noise rise, and the associated PFD or EPFD is obtained analytically. The resulting limits are then associated with the throughput degradation at the corresponding noise-rise level.

Same thermal-noise reference is used in both parts of the methodology. In the Monte Carlo calculation, $I_{ext} = N \cdot 10\hat{}(\rho/10)$ is added to I_{intra} N; in the PFD/EPFD conversion,

that identical I_{ext} is expressed as incident flux density. No correction based on the loaded-network I_{ext}/N is required, and the values of PFD limits obtained in this study correspond directly to the external interference levels used for the reported throughput-loss cases.

Figure 9 summarizes the victim-centric procedure. A candidate receiver noise rise, I_{ext}/N is applied to the exposed terrestrial receivers, and full-network throughput loss is calculated relative to the paired baseline. The highest evaluated grid point satisfying the 5% screening ceiling in all cases of the relevant direction is retained as a candidate protection level and converted to PFD or EPFD. The finite grid means that the procedure selects a tested case rather than solving an exact crossing point.

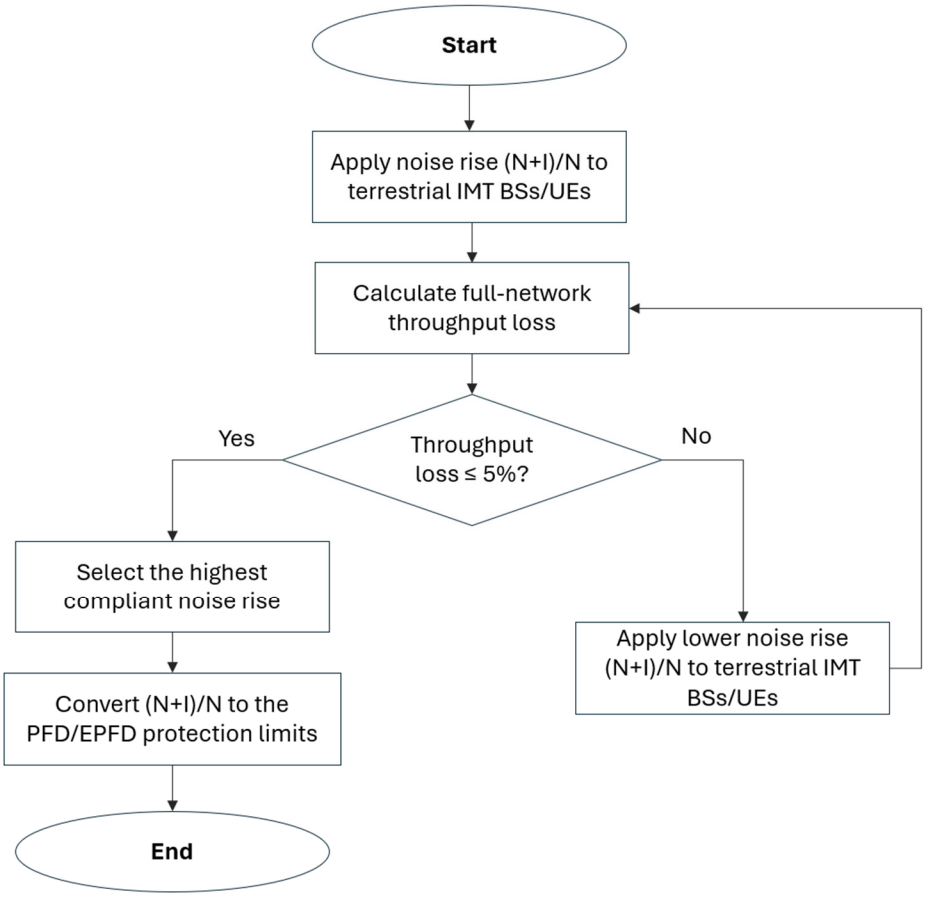


Figure 9. Victim-centric procedure for deriving NGSO-design-independent PFD/EPFD protection limits from the adopted 5% full-network throughput-loss criterion.

The receiver-side conversion does not prescribe an NGSO architecture, but the numerical throughput response is conditional on the assumed terrestrial deployment and exposure fractions. A D2C operator must use its actual constellation, beams, loading, propagation, and simultaneous emissions to demonstrate that the aggregate PFD or EPFD at the protected receiver does not exceed the applicable level.

3.7. Reference NGSO System and Resulting Exposure Statistics

The exposure assumptions used in Sections 4 and 5 are motivated by an explicit simulation of one reference direct-to-cell NGSO system submitted to ITU-R Working Party 4C; its parameters are reproduced in Table 5. The system is used only to characterize one set of receiver-exposure statistics.

Table 5. Parameters of the reference NGSO direct-to-cell system used to establish the exposure statistics, as submitted to ITU-R Working Party 4C under WRC-27 agenda item 1.13.

Parameter	Value
Orbital configuration	
Orbit type	Walker
Altitude	525 km
Inclination	53°
Number of orbital planes	28
Satellites per plane	120
Total number of satellites	3360
Space station transmitter	
Frequency range	2500–2690 MHz
Bandwidth per beam	5 MHz
Polarization	RHCP
Maximum power flux density	−83.5 dB(W/(m^2·MHz))
Antenna radiation pattern	Rec. ITU-R S.1528, Section 1.4 [21]
Maximum antenna gain, G_max	34.1 dBi
Antenna dimensions, L_r = L_t	1.6 m
Side-lobe ratio, SLR	20 dB
Pattern parameter, l	2
Wavelength, λ	0.15 m

Figure 10 shows a snapshot of the constellation, in which 3229 of the 3360 satellites are transmitting. Satellites whose sub-satellite point falls within a rectangular exclusion zone over the territory containing the terrestrial cluster are switched off, which represents the operational practice assumed for a system reusing terrestrial IMT spectrum by agreement with the administration concerned. Of the transmitting satellites, 91 are simultaneously visible from the cluster and therefore contribute to the aggregate interference at that instant.

Figure 11 gives the complementary cumulative distribution of the population-average I_{ext}/N produced by the reference system at outdoor and indoor UEs, with outdoor-to-indoor loss modeled according to Recommendation ITU-R P.2109 [19]. The two medians differ by 14.6 dB (−9.0 dB outdoors and −23.6 dB indoors). This result motivates, 50% exposed-UE assumption used in Section 4. This exposure generally is based on the information from Report ITU-R M.2292 [6] which says that 50% of the rural UEs are located indoors.

Figure 12 gives the corresponding distributions at the base-station receiver for three sectors with Recommendation ITU-R F.1336 patterns and 3 degrees mechanical downtilt. The sector medians are +1.6, −0.3, and −6.8 dB. Two of the three orientations therefore have medians above −6 dB; the 70% exposed-sector assumption is a rounded statistical representation of this two-of-three result for the reference geometry. It remains a scenario assumption rather than a universal property of NGSO systems.

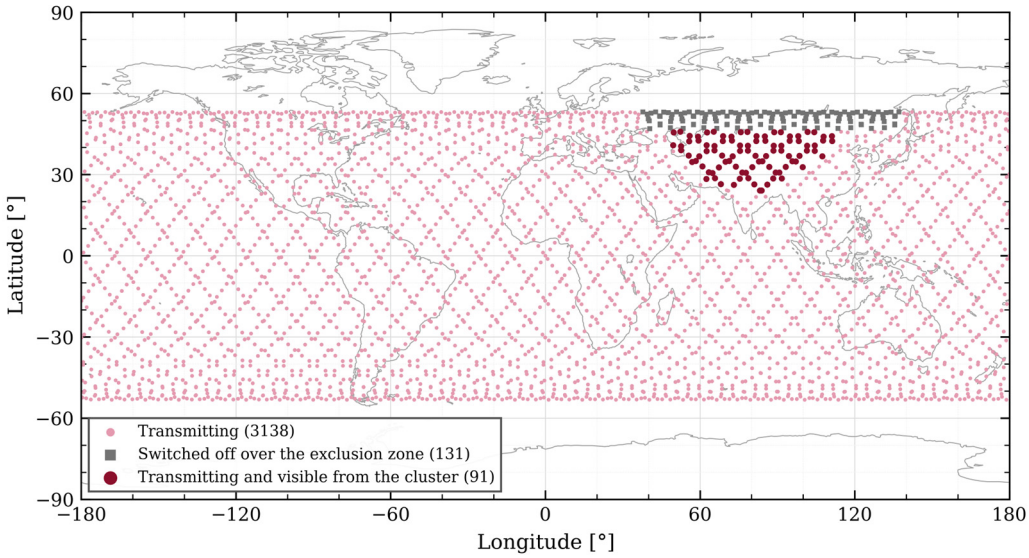


Figure 10. Snapshot of the reference NGSO constellation, showing transmitting satellites, satellites switched off over the exclusion zone, and satellites simultaneously transmitting and visible from the terrestrial cluster. Of the 3360 satellites, 3229 are transmitting at the instant shown and 91 are visible from the cluster.

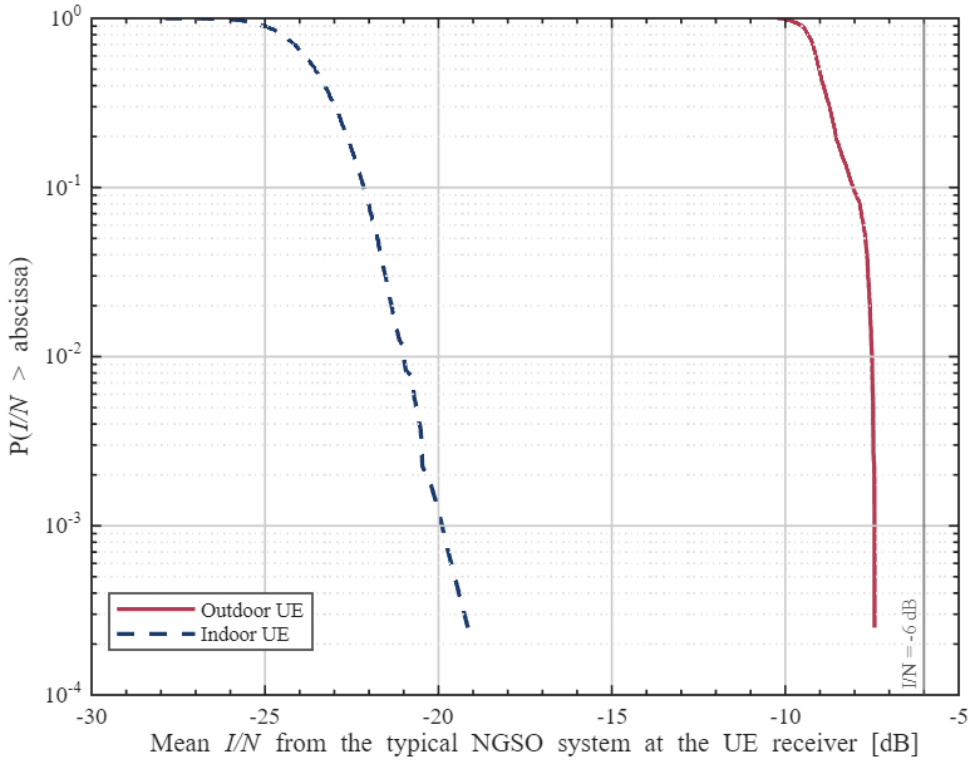


Figure 11. Complementary cumulative distribution of the population-average interference-to-noise ratio produced by the reference NGSO system at outdoor and indoor user equipment, downlink. Outdoor-to-indoor loss is modeled in accordance with Recommendation ITU-R P.2109 [19] and applied on the space-to-Earth path, with half of the user population located indoors. The vertical line marks the $I_{ext}/N = -6$ dB protection criterion.

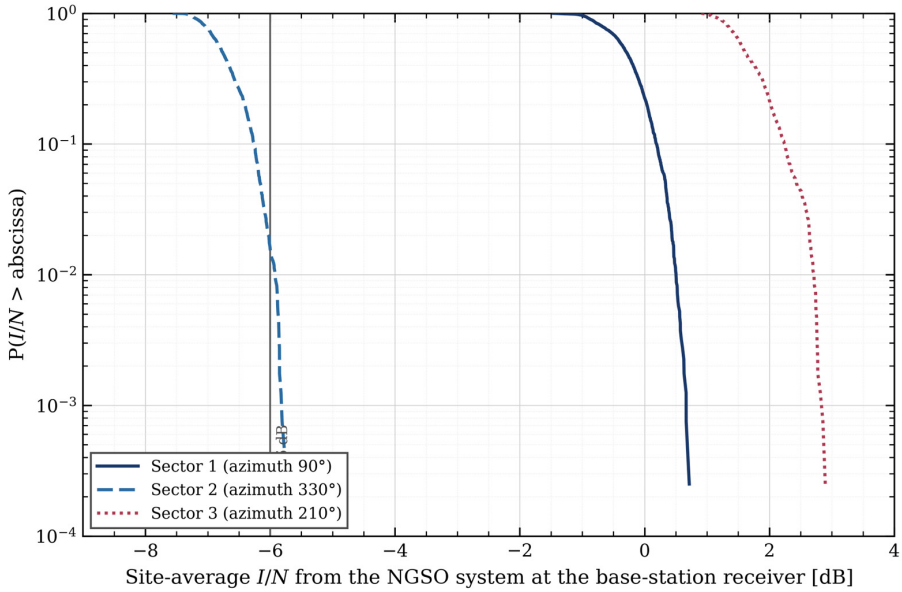


Figure 12. Complementary cumulative distribution of the site-average interference-to-noise ratio produced by the reference NGSO system at the base-station receiver, by sector. Base-station antenna patterns follow Recommendation ITU-R F.1336 with 3 degrees of mechanical downtilt. The vertical line marks the $I_{ext}/N = -6$ dB protection criterion.

4. Downlink Results and Protection of IMT User Equipment

4.1. Downlink Throughput Degradation

Figures 13–19 show the cumulative distribution functions (CDFs) of aggregate downlink cluster throughput for the 734, 852, 925, 1805, 1900, 2110, and 2620 MHz cases. In every band, increasing the prescribed receiver noise rise shifts the throughput distribution toward lower values. The black dashed curve gives the baseline without external interference, while the colored curves correspond to noise rises of 1.00, 1.19, 1.46, 1.76, and 3.00 dB.

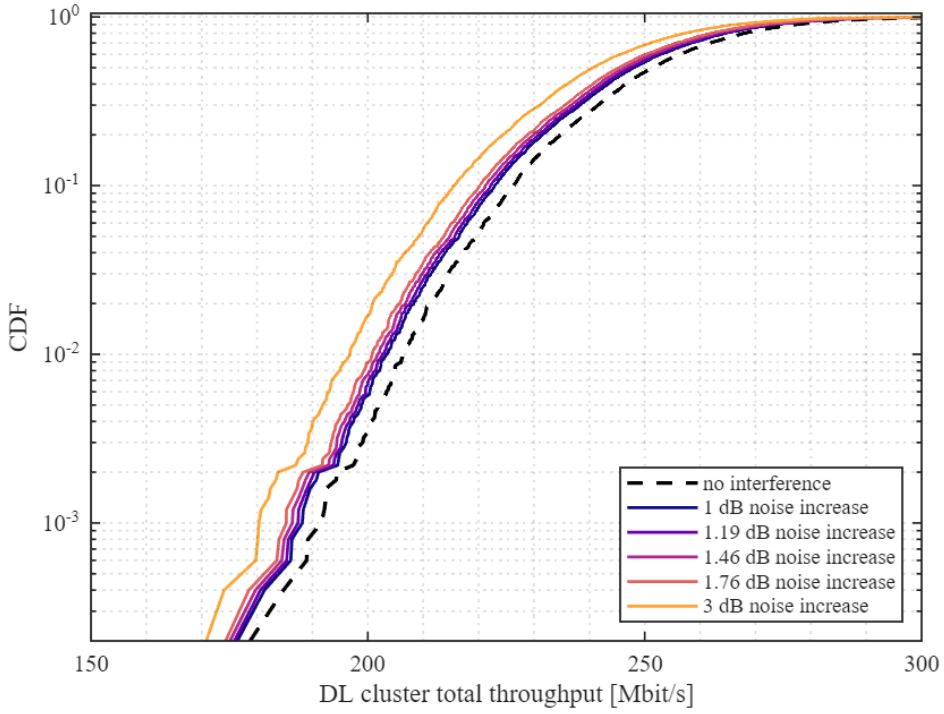


Figure 13. CDF of aggregate downlink cluster throughput at 734 MHz for the evaluated receiver noise-rise levels.

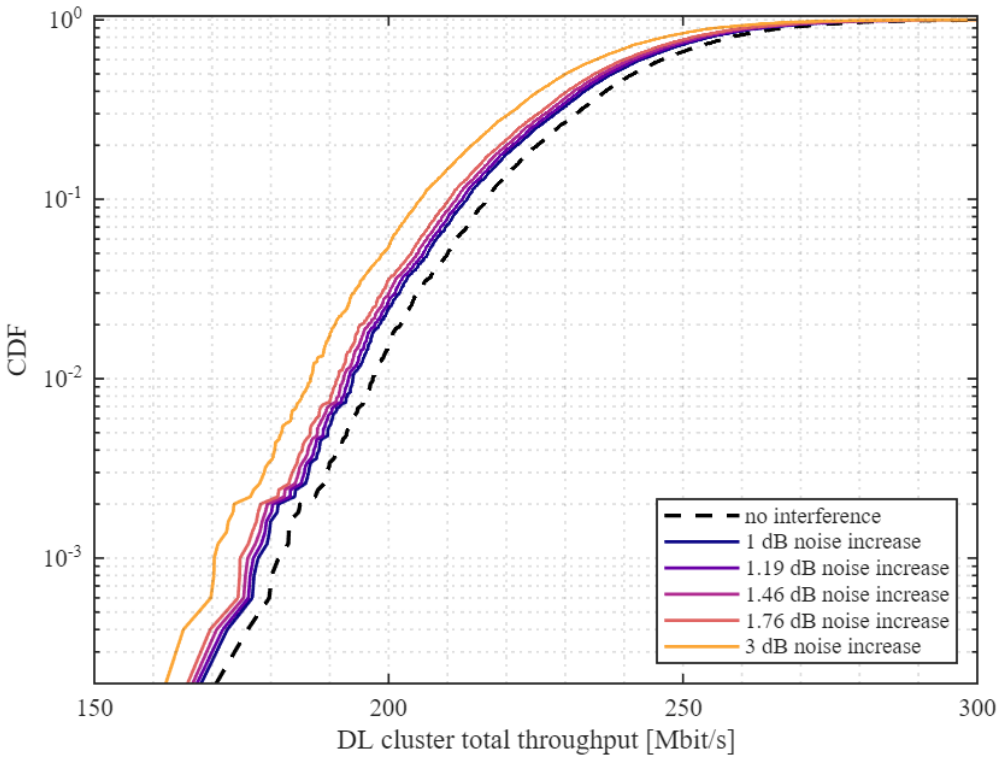


Figure 14. CDF of aggregate downlink cluster throughput at 852 MHz for the evaluated receiver noise-rise levels.

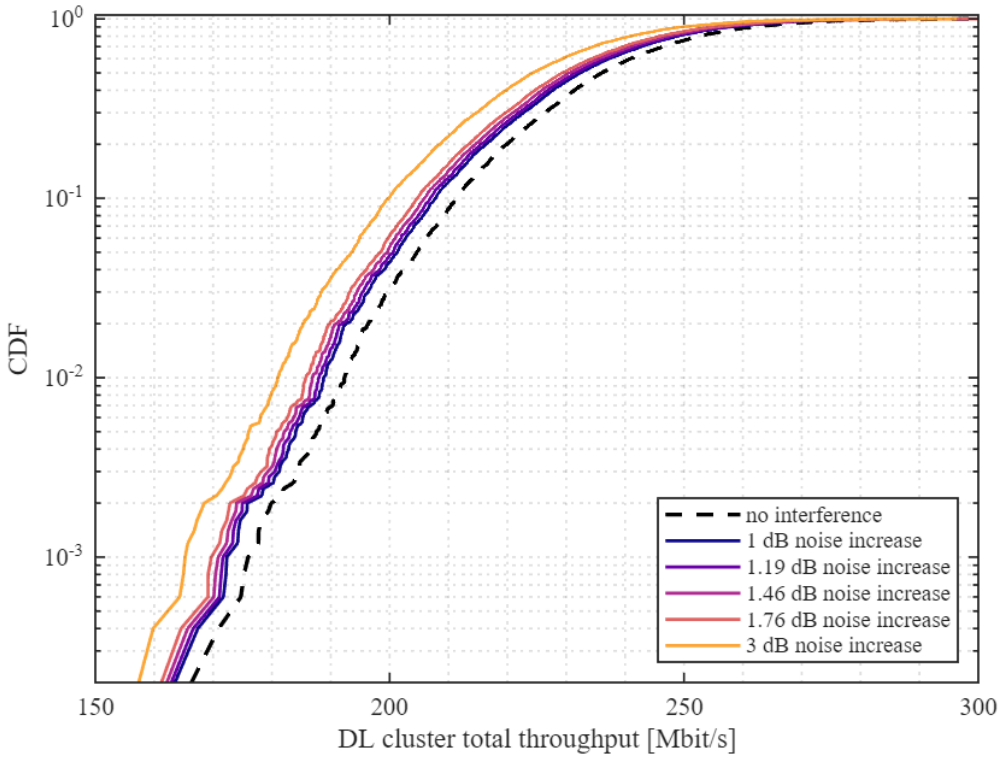


Figure 15. CDF of aggregate downlink cluster throughput at 925 MHz for the evaluated receiver noise-rise levels.

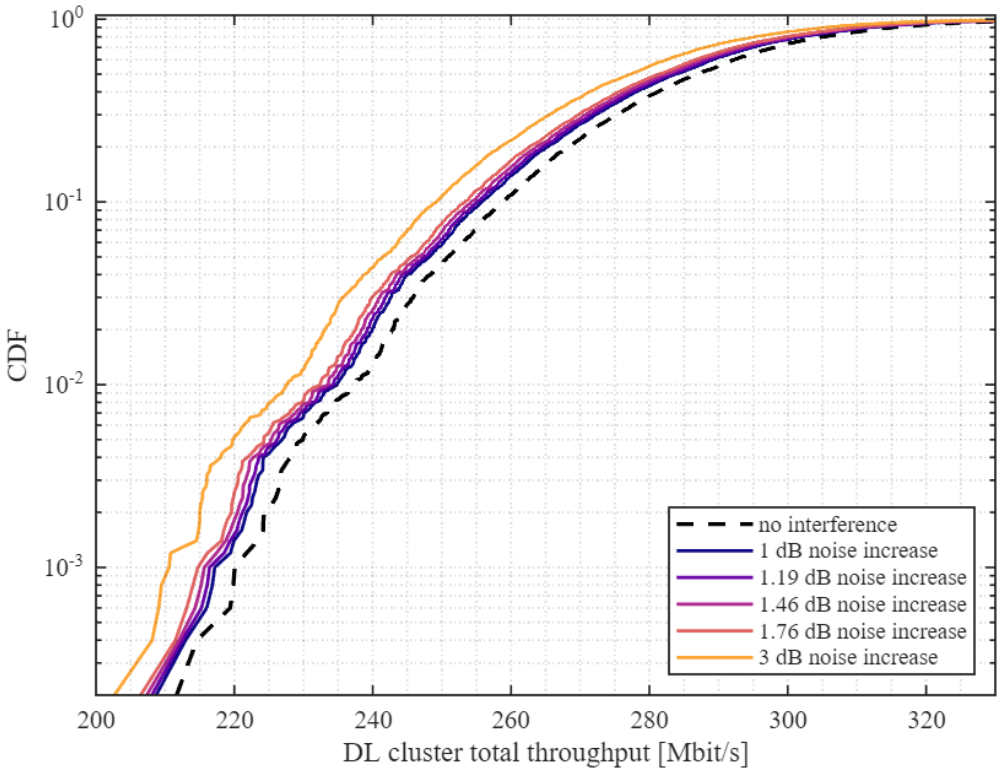


Figure 16. CDF of aggregate downlink cluster throughput at 1805 MHz for the evaluated receiver noise-rise levels.

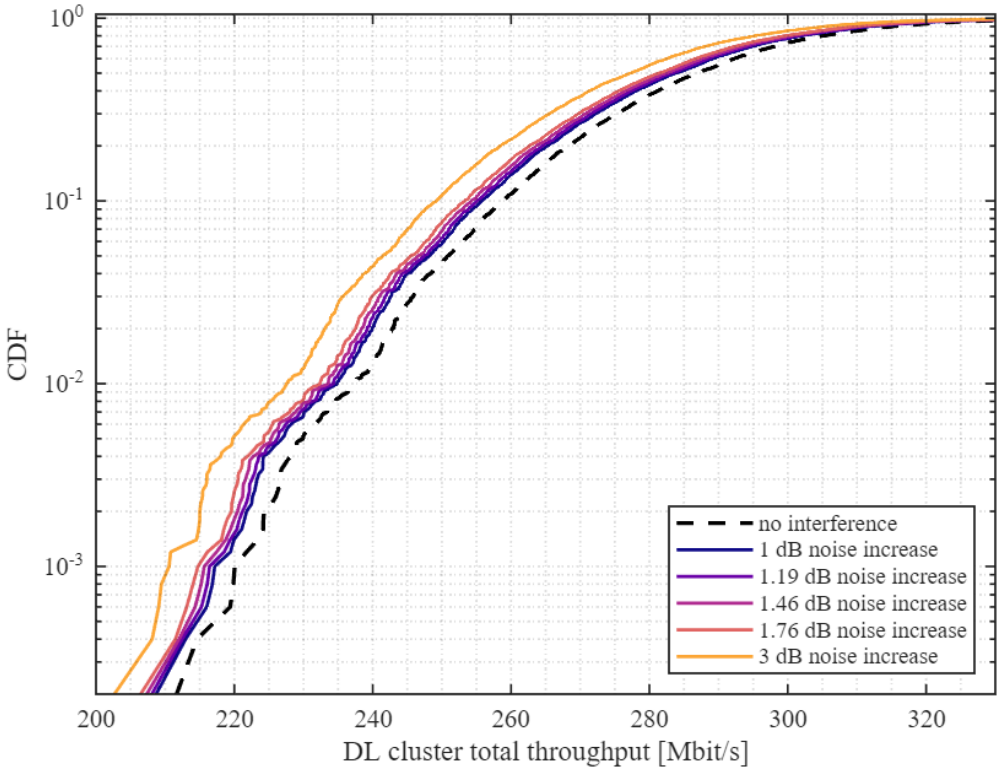


Figure 17. CDF of aggregate downlink cluster throughput at 1900 MHz for the evaluated receiver noise-rise levels.

https://doi.org/10.3390/network6030071

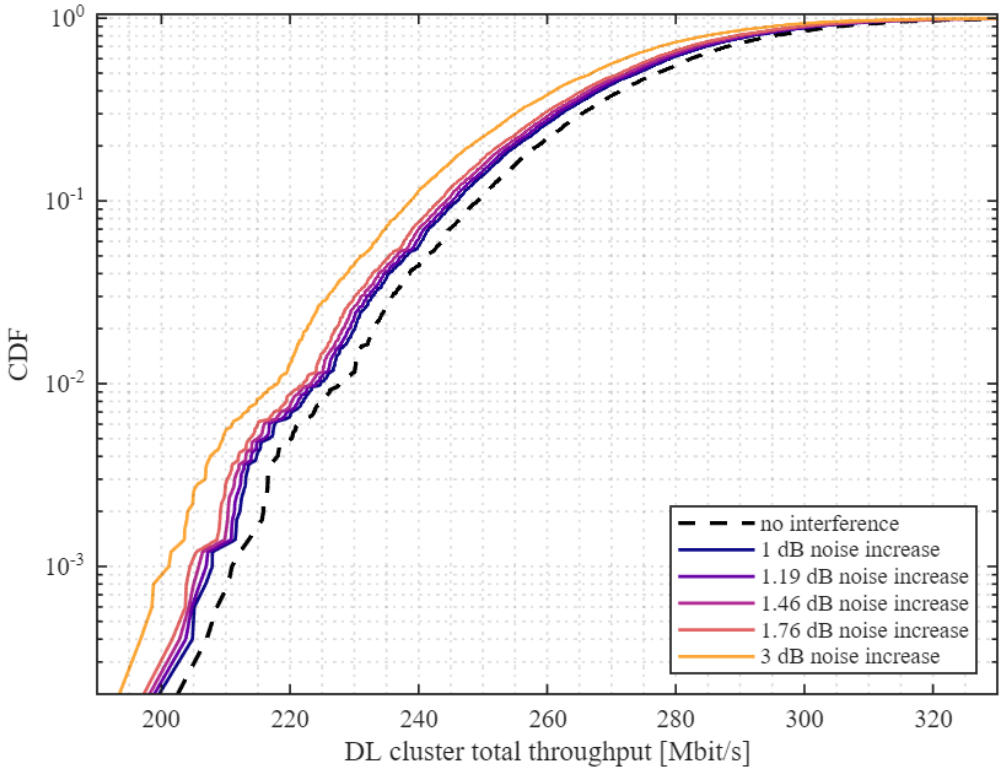


Figure 18. CDF of aggregate downlink cluster throughput at 2110 MHz for the evaluated receiver noise-rise levels.

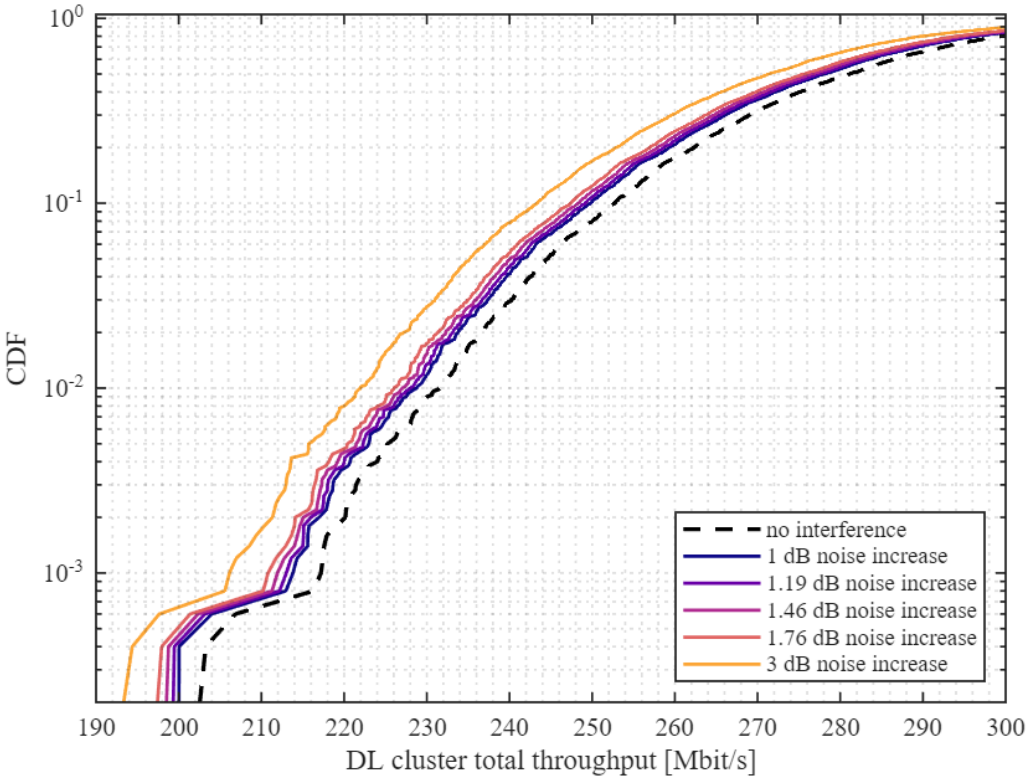


Figure 19. CDF of aggregate downlink cluster throughput at 2620 MHz for the evaluated receiver noise-rise levels.

Tables 6 and 7 summarize the downlink throughput losses for the reference cell and the full 57-cell network, respectively. At a 1 dB receiver noise rise, the reported loss ranges

from 1.25% to 1.82% for the reference cell and from 1.04% to 1.53% for the network. At a 3 dB noise rise, the corresponding ranges increase to 4.01–5.80% and 3.39–4.95%. The largest 3 dB losses occur in the frequency cases below 1 GHz.

Table 6. Downlink throughput loss in the reference cell for the evaluated receiver noise-rise levels.

Frequency	$(N + I_{ext})/N$ = 1 dB $I_{ext}/N = -6$ dB	$(N + I_{ext})/N$ = 1.19 dB $I_{ext}/N = -5$ dB	$(N + I_{ext})/N$ = 1.46 dB $I_{ext}/N = -4$ dB	$(N + I_{ext})/N$ = 1.76 dB $I_{ext}/N = -3$ dB	$(N + I_{ext})/N$ = 3 dB I_{ext}/N = 0 dB
734 MHz	1.56%	1.93%	2.36%	2.88%	5.04%
852 MHz	1.73%	2.12%	2.61%	3.18%	5.53%
925 MHz	1.82%	2.24%	2.74%	3.34%	5.8%
1805 MHz	1.25%	1.54%	1.89%	2.3%	4.01%
1900 MHz	1.26%	1.55%	1.9%	2.31%	4.13%
2110 MHz	1.26%	1.58%	2.05%	2.4%	4.24%
2620 MHz	1.27%	1.57%	1.92%	2.34%	4.09%

Table 7. Downlink throughput loss in the full 57-cell network for the evaluated receiver noise-rise levels.

Frequency	$(N + I_{ext})/N$ = 1 dB $I_{ext}/N = -6$ dB	$(N + I_{ext})/N$ = 1.19 dB $I_{ext}/N = -5$ dB	$(N + I_{ext})/N$ = 1.46 dB $I_{ext}/N = -4$ dB	$(N + I_{ext})/N$ = 1.76 dB $I_{ext}/N = -3$ dB	$(N + I_{ext})/N$ = 3 dB I_{ext}/N = 0 dB
734 MHz	1.3%	1.61%	1.98%	2.41%	4.25%
852 MHz	1.45%	1.79%	2.2%	2.68%	4.7%
925 MHz	1.53%	1.89%	2.32%	2.83%	4.95%
1805 MHz	1.05%	1.3%	1.59%	1.95%	3.42%
1900 MHz	1.05%	1.34%	1.59%	1.94%	3.55%
2110 MHz	1.04%	1.44%	1.67%	2.06%	3.68%
2620 MHz	1.04%	1.29%	1.58%	1.93%	3.39%

4.2. PFD Limits for UE Protection

Table 8 gives the PFD levels obtained by selecting the 3 dB receiver noise-rise case and normalizing the result to a 1 MHz reference bandwidth. The levels range from −109.23 dB(W/(m^2·MHz)) at 734 MHz to −98.17 dB(W/(m^2·MHz)) at 2620 MHz.

Table 8. PFD limits for protection of terrestrial IMT user equipment, derived using the performance-based 3 dB receiver noise-rise criterion.

Frequency	PFD Limit [dB(W/(m^2·MHz))]
734 MHz	−109.23
852 MHz	−107.93
925 MHz	−107.22
1805 MHz	−101.41
1900 MHz	−100.97
2110 MHz	−100.10
2620 MHz	−98.17

Under the assumptions of this study, the tested 0 dB I_{ext}/N case gives network-wide downlink loss of 3.39–4.95 and is therefore retained as a candidate level under the 5% screening rule. The result is conditional on 50% UE exposure and on the finite 57-cell

deployment. It is not an exact estimate of the maximum tolerable interference. The conventional $I_{ext}/N = -6$ dB case gives lower modeled loss (1.04–1.82%) and would provide an additional 6 dB margin relative to the selected tested case.

5. Uplink Results and Protection of IMT Base Stations

5.1. EPFD Formulation

Protection of terrestrial IMT base stations is expressed in terms of EPFD so that the directional receiving gain of the base-station antenna is incorporated. Article 22 of Radio Regulations [22] defines the equivalent power flux-density as follows:

$$\mathrm{EPFD} = 10\log_{10}\left[\sum_{i=1}^{N_a} 10^{P_i/10}\frac{G_t(\theta_i)}{4\pi d_i^2}\frac{G_r(\varphi_i)}{G_{r,\max}}\right] \tag{11}$$

Here, P_i is expressed in dBW in the reference bandwidth, while the antenna gains inside the summation are linear ratios. Article 22 therefore treats EPFD as the aggregate power flux density from all visible interfering transmitters, weighted by the off-axis discrimination of the reference receiving antenna.

Define the ordinary power flux density produced by transmitter i as follows:

$$S_i = 10^{P_i/10}\frac{G_t(\theta_i)}{4\pi d_i^2} \qquad \left[\mathrm{W/m^2}\right] \tag{12}$$

The Article 22 equation in linear units is then as follows:

$$\mathrm{epfd_{lin}} = \sum_{i=1}^{N_a} S_i\frac{G_r(\varphi_i)}{G_{r,\max}}. \tag{13}$$

The effective aperture of the receiving antenna in direction φ_i is as follows:

$$A_e(\varphi_i) = \frac{\lambda^2}{4\pi}G_r(\varphi_i) \tag{14}$$

The aggregate interference power at the antenna is as follows:

$$I_{\mathrm{ant}} = \sum_{i=1}^{N_a} S_i A_e(\varphi_i) = \sum_{i=1}^{N_a} S_i\frac{\lambda^2}{4\pi}G_r(\varphi_i) \tag{15}$$

Factoring out the maximum receiving-antenna gain gives the following:

$$I_{\mathrm{ant}} = \frac{\lambda^2}{4\pi}G_{r,\max}\sum_{i=1}^{N_a} S_i\frac{G_r(\varphi_i)}{G_{r,\max}}. \tag{16}$$

The summation is exactly the linear EPFD. Consequently, the expression below can express I_{ant}:

$$I_{\mathrm{ant}} = \mathrm{epfd_{lin}}\frac{\lambda^2}{4\pi}G_{r,\max}, \tag{17}$$

and therefore the following:

$$\mathrm{epfd_{lin}} = \frac{I_{\mathrm{ant}}}{G_{r,\max}\lambda^2/(4\pi)}. \tag{18}$$

The denominator is the maximum effective aperture of the reference receiving antenna:

$$A_{e,\max} = G_{r,\max}\frac{\lambda^2}{4\pi}. \tag{19}$$

In dB, that would have the following form:

$$\mathrm{EPFD} = I_{\mathrm{ant}} - G_{\max} - 10\log_{10}\left(\frac{\lambda^2}{4\pi}\right) \tag{20}$$

Here, EPFD is expressed in dB(W/m^2) in the applicable reference bandwidth; I_{ant} is expressed in dBW in the same reference bandwidth; G_{max} is expressed in dBi; and λ is expressed in meters. With feeder loss it would be as follows:

$$\mathrm{EPFD} = I_{\mathrm{rx}} + L_{\mathrm{feeder}} - G_{\max} - 10\log_{10}\left(\frac{\lambda^2}{4\pi}\right) \tag{21}$$

The feeder-loss term has a positive sign because a larger EPFD is required at the antenna to produce the same permissible interference power after attenuation in the feeder.

Hence, the EPFD limit would be as follows:

$$\mathrm{EPFD}_{\mathrm{lim}} = 10\log_{10}(kT_0B) + NF + \left(\frac{I}{N}\right)_{\mathrm{lim,dB}} - G_{\max} + L_{\mathrm{feeder}} - 10\log_{10}\left(\frac{\lambda^2}{4\pi}\right) \tag{22}$$

Converting I/N to (N + I)/N will give the following equation:

$$\mathrm{EPFD}_{\mathrm{lim}} = 10log_{10}(kT_0B) + \mathrm{NF} + 10log_{10}\left(10^{\frac{(N+I_{ext})/N}{10}} - 1\right) - G_{max} + L_{feeder} - 10log_{10}\left(\frac{\lambda^2}{4\pi}\right) \tag{23}$$

where the following applies:

k: Boltzmann's constant (1.380649×10^{-23} J/K);
T_0: receiver thermal noise in K;
B: reference bandwidth (1 MHz);
NF: receiver noise figure in dB;
$(N + I_{ext})/N$: thermal-noise rise corresponding to the applied external interference in dB;
G_{max}: effective maximum antenna gain of BS in dBi;
θ: the elevation angle;
L_{feeder}: Receiver antenna feeder loss for IMT BS.

EPFD weights each simultaneously incident PFD contribution by the base-station receive gain in its direction of arrival and combines the weighted contributions in the linear domain before conversion to decibels. The values reported here are aggregate system levels: the summation includes all simultaneously visible satellites and active beams of one NGSO system. Aggregate interference from multiple independent D2C systems is outside the present scope. For AAS, the dynamically changing receive gain requires the time-dependent statistical compliance methodology identified in Section 6.

5.2. Uplink Throughput Degradation

Figures 20–23 show the CDFs of aggregate uplink cluster throughput for the 734, 852, 1900, and 2620 MHz cases. As in the downlink, increasing the receiver noise rise shifts the distributions toward lower throughput. The numerical results show that the uplink degradation is more pronounced than the downlink degradation for the same nominal noise-rise values, reflecting the different uplink link budgets and terrestrial interference conditions.

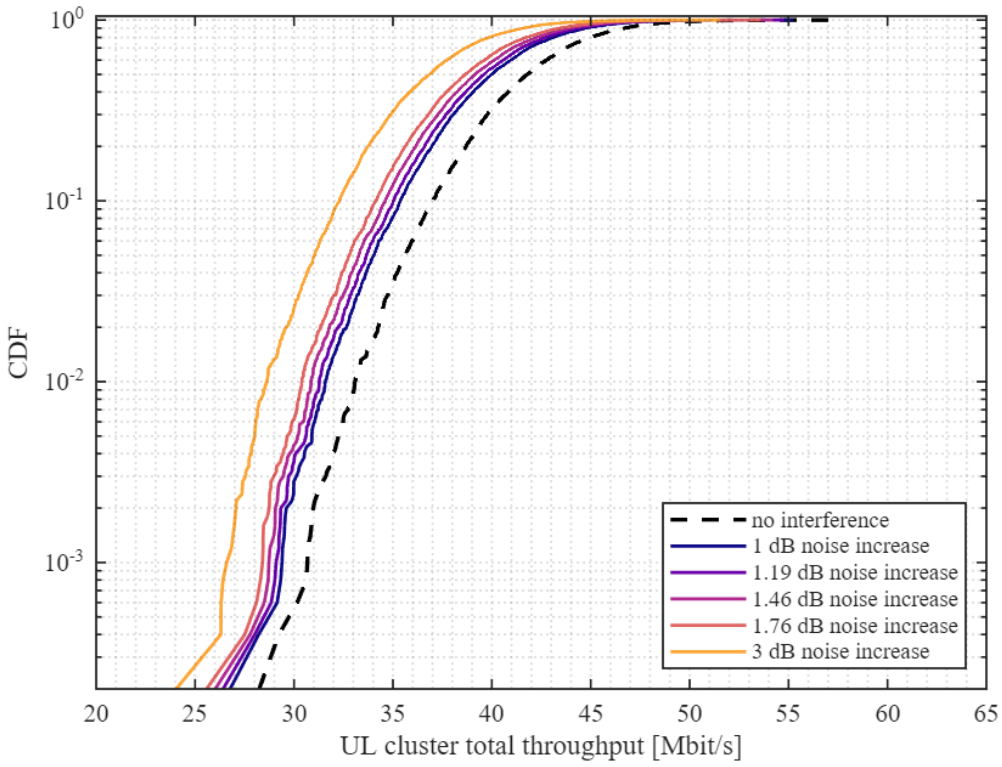


Figure 20. CDF of aggregate uplink cluster throughput at 734 MHz for the evaluated receiver noise-rise levels.

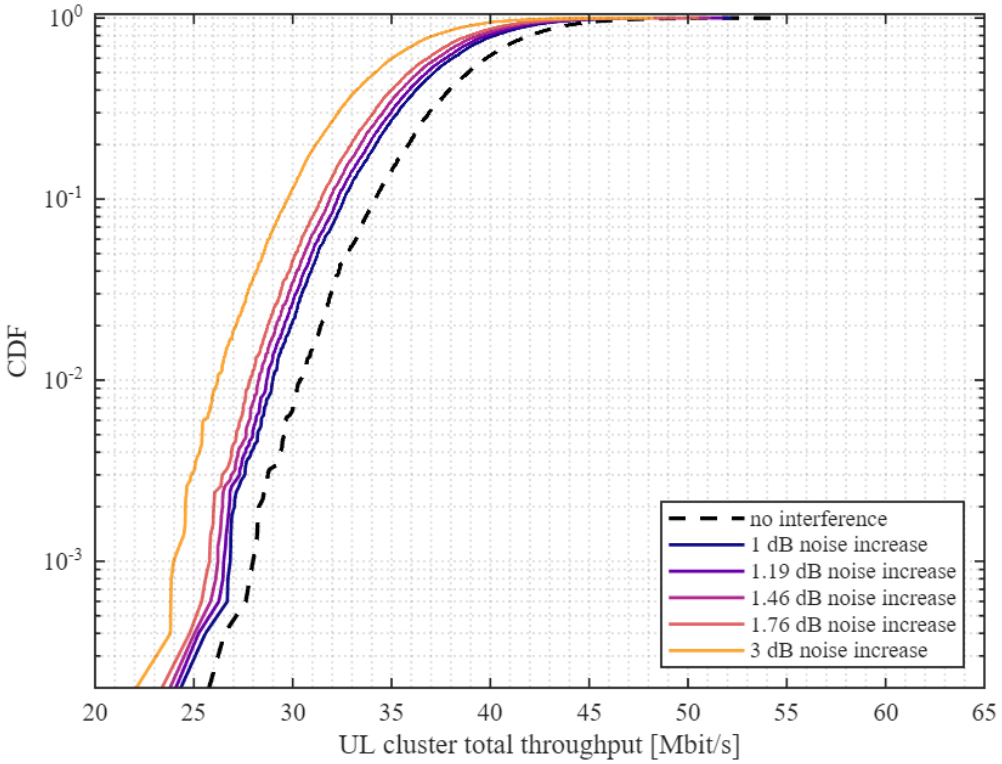


Figure 21. CDF of aggregate uplink cluster throughput at 852 MHz for the evaluated receiver noise-rise levels.

https://doi.org/10.3390/network6030071

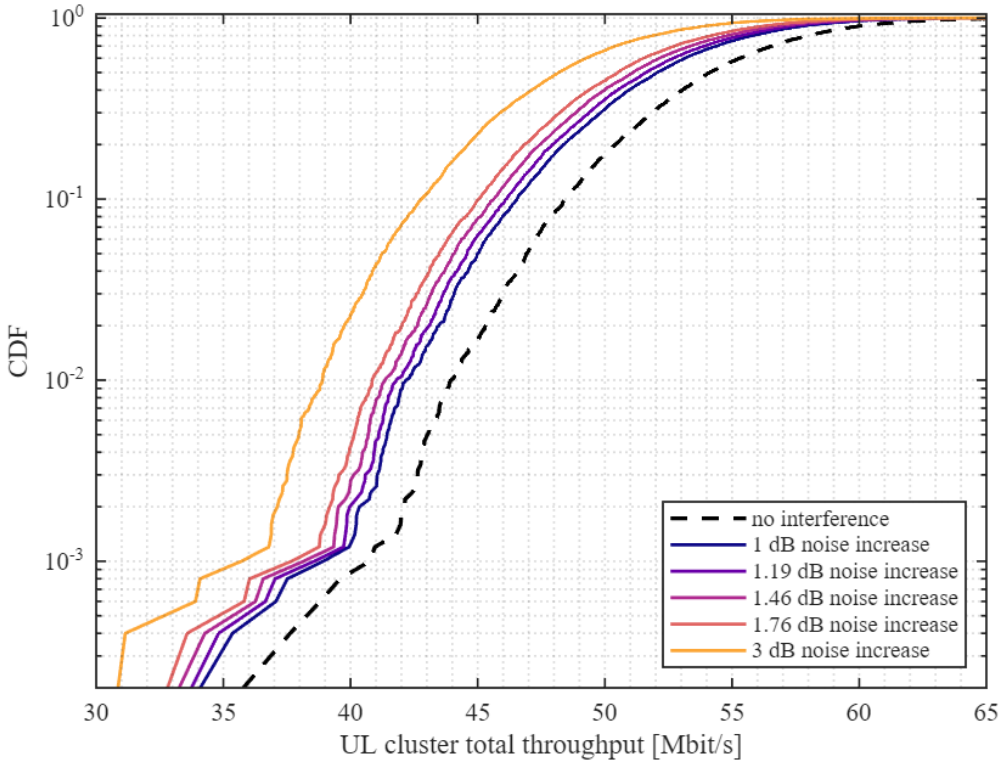


Figure 22. CDF of aggregate uplink cluster throughput at 1900 MHz for the evaluated receiver noise-rise levels.

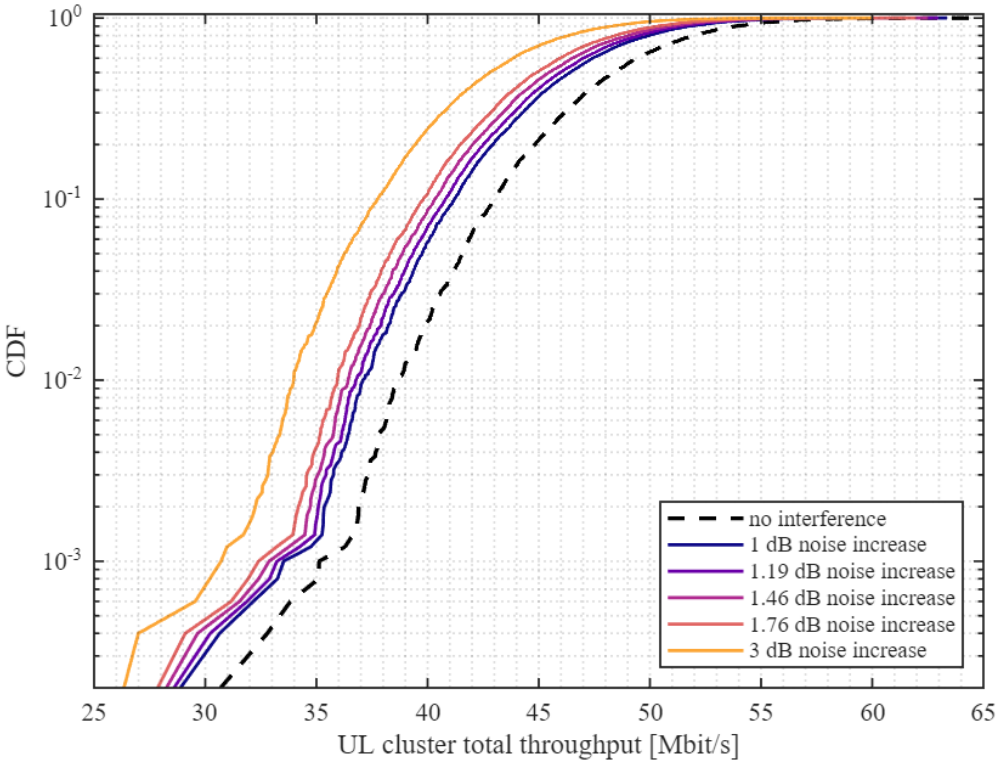


Figure 23. CDF of aggregate uplink cluster throughput at 2620 MHz for the evaluated receiver noise-rise levels.

Tables 9 and 10 summarize the uplink throughput losses for the full 57-cell network and the reference cell, respectively. At a 1 dB receiver noise rise, the loss ranges from 4.13% to 4.54% for the network and from 3.86% to 4.34% for the reference cell. At a 1.19 dB noise

rise, the corresponding ranges are 5.01–5.49% and 4.70–5.27%, showing that the network-wide 5% ceiling is already crossed. At a 3 dB noise rise, the ranges increase to 11.53–12.43% and 10.98–12.05%, respectively. The uplink is therefore substantially more sensitive than the downlink to the same nominal receiver noise rise in the simulated scenarios.

Table 9. Uplink throughput loss in the full 57-cell network for the evaluated receiver noise-rise levels.

Frequency	$(N + I_{ext})/N$ = 1 dB $I_{ext}/N = -6$ dB	$(N + I_{ext})/N$ = 1.19 dB $I_{ext}/N = -5$ dB	$(N + I_{ext})/N$ = 1.46 dB $I_{ext}/N = -4$ dB	$(N + I_{ext})/N$ = 1.76 dB $I_{ext}/N = -3$ dB	$(N + I_{ext})/N$ = 3 dB I_{ext}/N = 0 dB
734 MHz	4.5%	5.44%	6.56%	7.79%	12.32%
852 MHz	4.54%	5.49%	6.6%	7.87%	12.43%
1900 MHz	4.13%	5.01%	6.04%	7.21%	11.53%
2620 MHz	4.25%	5.15%	5.93%	7.4%	11.8%

Table 10. Uplink throughput loss in the reference cell for the evaluated receiver noise-rise levels.

Frequency	$(N + I_{ext})/N$ = 1 dB $I_{ext}/N = -6$ dB	$(N + I_{ext})/N$ = 1.19 dB $I_{ext}/N = -5$ dB	$(N + I_{ext})/N$ = 1.46 dB $I_{ext}/N = -4$ dB	$(N + I_{ext})/N$ = 1.76 dB $I_{ext}/N = -3$ dB	$(N + I_{ext})/N$ = 3 dB I_{ext}/N = 0 dB
734 MHz	4.27%	5.17%	6.23%	7.43%	11.87%
852 MHz	4.34%	5.27%	6.34%	7.57%	12.05%
1900 MHz	3.86%	4.7%	5.67%	6.79%	10.98%
2620 MHz	4.05%	4.92%	6.2%	7.09%	11.39%

5.3. Derived EPFD Limits and Cross-Border Applicability

Table 11 presents aggregate candidate EPFD levels derived from $I_{ext}/N = -6$ dB. For non-AAS base stations, the level varies from −138.23 to −130.18 dB(W/(m^2·MHz)). At 1900 MHz, the AAS value is 11.2 dB more stringent than the non-AAS value because the EPFD conversion is normalized by the higher maximum AAS receive gain.

Table 11. EPFD limits for protection of terrestrial IMT base stations, derived using $I_{ext}/N = -6$ dB.

Frequency and Antenna Configuration	EPFD Limit [dB(W/(m^2·MHz))]
734 MHz non-AAS	−138.23
852 MHz non-AAS	−136.93
1900 MHz non-AAS	−132.97
2620 MHz non-AAS	−130.18
1900 MHz AAS	−144.17
2620 MHz AAS	−141.37

The 11.2 dB offset is therefore a normalization consequence and must not be interpreted as evidence that AAS sites experience greater incident satellite exposure. It is also compatible with the lower median terrestrial intra-network interference observed for AAS in Figure 8, because that distribution and the EPFD maximum-gain normalization describe different quantities. Compliance must be evaluated using the applicable directional gain model and the linear aggregation in Section 5.1.

All evaluated network-wide uplink losses remain below 5% at $I_{ext}/N = -6$ dB, whereas the next tested grid point, −5 dB, gives 5.01–5.49%. The −6 dB case is consequently retained as a conservative tested candidate consistent with the conventional receiver criterion; no exact 5% crossing is claimed.

The base-station limits represent a worst-case cross-border condition in which neighboring countries operate the same spectrum in opposite transmission directions. Administrations commonly seek to harmonize FDD and TDD arrangements, so the applicability of the base-station EPFD limits depends on the frequency plans actually used on the two sides of a border.

Consequently, studies and regulatory provisions under WRC-27 agenda item 1.13 should distinguish between same-direction and opposite-direction cross-border operation. The EPFD limits derived here are relevant to the latter case and should not be applied indiscriminately where the terrestrial frequency arrangements do not expose base-station receivers to satellite downlink emissions.

6. Discussion

6.1. Direction-Dependent Results and Regulatory Interpretation

The results demonstrate that a common external I_{ext}/N value does not produce the same network-level effect in the downlink and uplink. At the displayed 1 dB thermal-noise rise, downlink throughput loss lies between 1.04% and 1.82%, whereas uplink loss lies between 3.86% and 4.54%. At the displayed 3 dB rise, downlink loss increases to 3.39–5.80% and uplink loss to 10.98–12.43%. The greater uplink sensitivity reflects the different baseline I_{intra}/N regimes at the base-station receiver.

This difference supports direction-specific tested candidate levels. For downlink, the 0 dB I_{ext}/N grid point remains below the 5% full-network screening ceiling in all seven evaluated cases. For uplink, the −6 dB grid point remains below the ceiling, while the next point (−5 dB) exceeds it in all four network-wide cases. These selections are conditional on the exposure fractions and finite deployment and do not estimate exact performance boundaries.

The paired reporting scopes are complementary. For each configuration, the reference cell is the outer-ring sector with the lowest mean downlink intra-network interference, selected from the completed Monte Carlo run. The full 57-cell result is the primary aggregate-impact metric. Because no wrap-around is used, boundary sectors have fewer interferers than an infinite deployment, so both scopes remain conditional on the finite-cluster geometry.

This distinction is especially important for the WRC-27 agenda item 1.13 scenario. The NR-NTN bands standardized by 3GPP to date are MSS allocations that are separate from terrestrial IMT operation [1–3]. By contrast, the scenario studied here reuses a spectrum identified for terrestrial IMT and already employed by LTE/5G networks, enabling satellite connectivity to unmodified smartphones [4]. Co-channel coexistence must therefore be evaluated for the terrestrial transmission direction actually used in each country.

For UE protection, the evaluated $I_{ext}/N = 0$ dB case gives candidate PFD levels from −109.23 to −98.17 dB(W/(m^2·MHz)) and modeled network-wide loss of 3.39–4.95%. For base-station protection, $I_{ext}/N = -6$ dB gives non-AAS candidate EPFD levels from −138.23 to −130.18 dB(W/(m^2·MHz)). The approximately 11 dB AAS/non-AAS difference at 1900 and 2620 MHz follows from maximum-gain normalization in the EPFD definition, not from a claim of greater AAS exposure.

The findings complement earlier band-specific interference analyses for direct-to-cell NTN operation [9,10], dynamic spectrum-coordination studies [11], and experimental receiver-desensitization measurements [12]. The present work extends those contributions by applying a common multi-cell methodology over several IMT bands, translating receiver degradation into network throughput loss, and then linking that loss to PFD and EPFD values. Dynamic coordination, beam management, or geographic exclusion mechanisms

can be treated as complementary mitigation measures, with the limits derived here serving as protection constraints for their design.

6.2. Scope, Compliance, and Limitations

The principal regulatory value of the methodology is this separation of responsibilities. The terrestrial study determines, once for each victim type, frequency band, antenna configuration, and sharing direction, the PFD or EPFD associated with the accepted performance degradation. An NGSO operator then models its own system only to determine whether its aggregate emissions at the protected IMT receiver comply with that limit. Because the compliance test is expressed at the receiver rather than in terms of a prescribed constellation design, systems with different numbers of satellites and beams, frequency-reuse patterns, power-control strategies, loading conditions, and operating modes can be assessed on the same basis. Simulating a single nominal NGSO system could not provide this common regulatory framework for protection of terrestrial systems. This division of responsibility is itself long established for flux-density limits; the contribution here is that the value of the limit is anchored to a measured network-performance criterion, so that its degree of conservatism can be stated explicitly rather than inherited from convention.

An important qualification concerns EPFD compliance for AAS BS. The AAS EPFD values reported in this study are receiver-protection targets derived using the assumed antenna characteristics; they do not by themselves constitute a complete operational compliance-verification method for a live AAS network. Unlike a non-AAS receiver with a fixed or slowly varying antenna pattern, an AAS base station continuously changes its beamforming weights and active beams as users, traffic, scheduling decisions, and resource-block allocations change. At the same time, a D2C (DC-MSS-IMT) satellite moves through azimuth and elevation. The receive gain of the AAS toward the interfering satellite is therefore time-, direction-, frequency-, and scheduler-dependent and cannot be represented reliably by one static gain value. Consequently, actual AAS EPFD compliance cannot be established by a purely static analytical conversion of PFD using a single assumed antenna gain.

The cross-border applicability of the EPFD limits must nevertheless be assessed using the frequency arrangements actually implemented by neighboring administrations. The most demanding base-station case occurs when satellite downlink emissions overlap terrestrial uplink reception because different countries use opposite transmission directions in the same spectrum. Where frequency plans are harmonized and the same direction is used on both sides of the border, the relevant victim receiver and required protection mechanism may be different. Regulatory provisions should therefore distinguish same-direction and opposite-direction cases rather than applying the most restrictive EPFD limit uniformly to every border.

Two assumptions tend to increase the modeled sensitivity. First, the three eight-RB scheduling chunks are continuously occupied in every cell; 24 of the 25 available RBs are allocated in each snapshot. Second, round-robin scheduling assigns equal RB chunks without exploiting instantaneous channel quality. These full-scheduled-load, non-opportunistic assumptions follow the convention used in Recommendation ITU-R M.2101 [5]. The resulting loss values should be interpreted as conditional high-load impacts rather than expected busy-hour predictions for all operational networks.

Several limitations define the scope of the candidate levels. The 50% UE and 70% base-station exposure fractions are fixed and motivated by one reference constellation at one geometry; no exposure-fraction sensitivity sweep was performed. Only five discrete I_{ext}/N points were tested, so the exact 5% crossing was not solved. A 95% confidence interval and convergence trace are shown for one representative downlink case, not for every band and direction. The terrestrial analysis uses one 6 km and 12 km inter-site-

distance RMa deployment, 5 MHz bandwidth, K = 3 simultaneously scheduled UEs per cell, one scheduler, and one set of antenna and power-control parameters. No wrap-around replication is used, so boundary sectors can bias the network average toward higher SINR and lower loss. The results therefore provide conditional tested candidate levels and not universal or statistically exact protection boundaries.

6.3. Further Research

A priority topic for further research is a reproducible methodology for verifying EPFD compliance at AAS base stations. Such a method should couple time-dependent NGSO ephemerides and incident PFD from all simultaneously visible satellites and active beams with the terrestrial AAS state, including UE locations, traffic load, scheduler decisions, beam codebooks, digital and analog beamforming weights, array calibration, and resource-block occupancy. For every time-frequency sample, the instantaneous AAS receive gain toward each interfering satellite should be obtained from a validated array model or measured antenna pattern. The interference contributions received should then be combined in the linear domain to obtain an EPFD time series or distribution. Compliance should be assessed against specified spatial and temporal percentiles, averaging intervals, and exceedance probabilities rather than against one nominal gain. Measurement campaigns, hardware-in-the-loop tests, and comparison with operational AAS beam logs would be needed to validate the methodology.

Additional research should examine aggregate interference from multiple D2C systems, simultaneous multi-beam operation, realistic frequency-reuse and power-control strategies, time-varying traffic loading, and mitigation measures such as beam blanking, power reduction, geographic exclusion, and dynamic coordination [11,23,24].

Dynamic coordination, beam management, geographic exclusion zones, and database-assisted coordination can be treated as complementary mitigation mechanisms for satellite–terrestrial spectrum sharing [11,24].

The terrestrial side should be extended to wrap-around deployments, urban and sub-urban channel models, wider bandwidths, different UE and base-station exposure fractions, and national FDD/TDD arrangements. In addition to mean throughput loss, future studies should evaluate cell-edge throughput, outage probability, latency, reliability, and service availability so that the selected regulatory criterion can be related to a broader set of IMT quality-of-service objectives. NGSO-specific studies should use actual constellation and propagation parameters to demonstrate compliance with the common limits, not to redefine terrestrial receiver tolerance separately for every constellation.

7. Conclusions

This study evaluated coexistence between terrestrial IMT networks and D2C satellite downlinks in frequency bands between 694/698 MHz and 2.7 GHz that are identified for terrestrial IMT and already used by LTE/5G systems. This spectrum-reuse scenario is distinct from existing 3GPP NR-NTN operation in dedicated MSS bands because it enables service to unmodified smartphones while creating co-channel interference risks for terrestrial UEs and, in opposite-direction cross-border cases, base stations.

A 57-cell terrestrial network with three simultaneously scheduled UEs per cell and a 5 MHz channel was evaluated over 5000 paired Monte Carlo snapshots. External interference was normalized to receiver thermal noise and added to $I_{intra} + N$ in the interfered SINR. It was applied to 50% of UEs in the downlink and 70% of base-station sectors in the uplink. The numerical results are therefore conditional on these exposure fractions and on the finite terrestrial deployment.

For downlink, the highest evaluated grid point, $I_{ext}/N = 0$ dB, gives network-wide loss of 3.39–4.95% and candidate PFD levels from −109.23 to −98.17 dB(W/(m^2·MHz)). For uplink, $I_{ext}/N = -6$ dB gives loss of 4.13–4.54%, while the next evaluated point gives 5.01–5.49%; the corresponding non-AAS candidate EPFD levels are −138.23 to −130.18 dB(W/(m^2·MHz)). These are conservative tested candidates under the adopted 5% screening rule, not exact estimates of a crossing point.

The results show that protection requirements depend on terrestrial link direction, receiver type, frequency, base-station antenna configuration, national frequency arrangements, and the assumed exposure model. Within a defined case, the receiver-side PFD or EPFD level can be used as a common compliance interface, while each operator models its actual aggregate NGSO emissions. The quantified mapping covers seven downlink frequency cases and four uplink frequency cases and demonstrates strong direction dependence. A complete AAS EPFD verification procedure and sensitivity studies over exposure fraction, wrap-around geometry, bandwidth, load, and scheduler remain for future work.

Author Contributions: Conceptualization, A.P. and V.T.; methodology, A.P.; software, A.P.; validation, V.T., A.P. and O.M.; formal analysis, A.P. and O.M.; investigation, V.T. and A.P.; resources, V.T. and A.P.; data curation, A.P. and O.M.; writing—original draft preparation, A.P.; writing—review and editing, V.T. and O.M.; visualization, A.P. and O.M.; supervision, V.T.; project administration, V.T.; funding acquisition, V.T. and A.P. All authors have read and agreed to the published version of the manuscript.

Funding: This research received no external funding.

Data Availability Statement: The original contributions presented in this study are included in the article. Further inquiries can be directed to the corresponding author.

Conflicts of Interest: The authors declare no conflicts of interest.

Abbreviations

The following abbreviations are used in this manuscript:

3GPP	Third Generation Partnership Project
AAS	Active antenna system
BS	Base station
CDF	Cumulative distribution function
D2C	Direct-to-cell satellite connectivity
DL	Downlink channel
EIRP	Equivalent isotropically radiated power
EPFD	Equivalent power flux density
FDD	Frequency division duplex
IoT	Internet of Things
IMT	International Mobile Telecommunications
ITU-R	International Telecommunication Union Radiocommunication Sector
TDD	Time division duplex
NTN	Non-Terrestrial Networks
NR	New Radio
MAC	Medium access control
MCL	Minimum coupling loss
MSS	Mobile Satellite Service
LTE	Long-Term Evolution
LEO	Low Earth orbit
SINR	Signal-to-interference-plus-noise ratio
PHY	Physical layer
PFD	Power flux density

RB	Resource Block
RHCP	Right-hand circular polarization
RMa	Rural Macro
UE	User equipment
UL	Uplink channel
WRC	World Radiocommunication Conference
DC-MSS-IMT	Direct connectivity between MSS space stations and IMT user equipment
NGSO	Non-geostationary satellite orbit
QAM	Quadrature amplitude modulation
QPSK	Quadrature phase-shift keying

References

1. Krause, J. *Non-Terrestrial Networks (NTN)*; 3GPP: Sophia Antipolis, France, 2024. Available online: https://www.3gpp.org/technologies/deep-dive/ntn-overview (accessed on 31 July 2026).
2. 3rd. Generation Partnership Project (3GPP). TR 38.863, Version 19.4.0, Release 19. In *Non-Terrestrial Networks (NTN) Related RF and Co-Existence Aspects*; 3GPP: Sophia Antipolis, France, 2026. Available online: https://portal.3gpp.org/desktopmodules/Specifications/SpecificationDetails.aspx?specificationId=3926 (accessed on 31 July 2026).
3. Panaitopol, D.; Jin, Y.; Tang, R.; Park, C. Requirements on Satellite Access Node and User Equipment for Non-Terrestrial Networks in 5G New Radio of 3GPP Release-17. *Int. J. Satell. Commun. Netw.* **2023**, *41*, 289–301. [CrossRef]
4. International Telecommunication Union (ITU). Resolution 253 (WRC-23): Studies on Possible New Allocations to the Mobile-Satellite Service for Direct Connectivity between Space Stations and International Mobile Telecommunications (IMT) User Equipment to Complement Terrestrial IMT Network Coverage. In *Final Acts of the World Radiocommunication Conference 2023*; ITU: Geneva, Switzerland, 2024; pp. 490–492.
5. International Telecommunication Union Radiocommunication Sector (ITU-R). *Recommendation ITU-R M.2101-0: Modelling and Simulation of IMT Networks and Systems for Use in Sharing and Compatibility Studies*; ITU: Geneva, Switzerland, 2017.
6. International Telecommunication Union Radiocommunication Sector (ITU-R). *Characteristics of Terrestrial IMT-Advanced Systems for Frequency Sharing/Interference Analyses*; ITU-R M.2292-0; ITU: Geneva, Switzerland, 2014. Available online: https://www.itu.int/pub/R-REP-M.2292-2014 (accessed on 20 July 2026).
7. International Telecommunication Union Radiocommunication Sector (ITU-R). *Recommendation ITU-R M.1036-8: Frequency Arrangements for Implementation of the Terrestrial Component of International Mobile Telecommunications in the Bands Identified for IMT in the Radio Regulations*; ITU: Geneva, Switzerland, 2026. Available online: https://www.itu.int/rec/R-REC-M.1036-8-202602-I/en (accessed on 23 July 2026).
8. Guidotti, A.; Vanelli-Coralli, A.; Conti, M.; Andrenacci, S.; Chatzinotas, S.; Maturo, N.; Evans, B.; Awoseyila, A.; Ugolini, A.; Foggi, T.; et al. Architectures and Key Technical Challenges for 5G Systems Incorporating Satellites. *IEEE Trans. Veh. Technol.* **2019**, *68*, 2624–2639. [CrossRef]
9. Pastukh, A.; Tikhvinskiy, V.; Devyatkin, E. Exploring Interference Issues in the Case of n25 Band Implementation for 5G/LTE Direct-to-Device NTN Services. *Sensors* **2024**, *24*, 1297. [CrossRef] [PubMed]
10. Pastukh, A.; Tikhvinskiy, V.; Dymkova, S.; Varlamov, O. Challenges of Using the L-Band and S-Band for Direct-to-Cellular Satellite 5G–6G NTN Systems. *Technologies* **2023**, *11*, 110. [CrossRef]
11. Martikainen, H.; Majamaa, M.; Puttonen, J. Coordinated Dynamic Spectrum Sharing between Terrestrial and Non-Terrestrial Networks in 5G and Beyond. In Proceedings of the 2023 IEEE 24th International Symposium on a World of Wireless, Mobile and Multimedia Networks (WoWMoM), Boston, MA, USA, 12–15 June 2023; pp. 419–424. [CrossRef]
12. Celidonio, M.; Consalvi, F. Co-Channel Interference from LEO Satellite Downlinks to 5G-NR Receivers in IMT Spectrum: An Experimental Study. *Electronics* **2026**, *15*, 2479. [CrossRef]
13. Lagunas, E.; Sharma, S.K.; Maleki, S.; Chatzinotas, S.; Ottersten, B. Resource Allocation for Cognitive Satellite Communications with Incumbent Terrestrial Networks. *IEEE Trans. Cogn. Commun. Netw.* **2015**, *1*, 305–317. [CrossRef]
14. Liu, L.; Li, Y.; Li, H.; Yang, J.; Liu, W.; Lan, J.; Wang, Y.; Li, J.; Wu, J.; Wu, Q.; et al. Democratizing Direct-to-Cell Low Earth Orbit Satellite Networks. In Proceedings of the 21st USENIX Symposium on Networked Systems Design and Implementation (NSDI'24), Santa Clara, CA, USA, 16–18 April 2024; pp. 791–808.
15. International Telecommunication Union Radiocommunication Sector (ITU-R). *Recommendation ITU-R F.1336-5: Reference Radiation Patterns of Omnidirectional, Sectoral and Other Antennas for the Fixed and Mobile Services for Use in Sharing Studies in the Frequency Range from 400 MHz to About 70 GHz*; ITU: Geneva, Switzerland, 2019. Available online: https://www.itu.int/rec/R-REC-F.1336-5-201901-I/en (accessed on 15 July 2026).

16. International Telecommunication Union Radiocommunication Sector (ITU-R). *Document 5D/716 of Chairman's Report Working Party 5D*; ITU: Geneva, Switzerland, 2021. Available online: https://www.itu.int/md/R19-WP5D-C-0716/en (accessed on 16 July 2026).
17. Generation Partnership Project (3GPP). *TR 36.942: Evolved Universal Terrestrial Radio Access (E-UTRA)*; Radio Frequency (RF) System Scenarios; 3GPP: Sophia Antipolis, France, 2025. Available online: https://www.etsi.org/deliver/etsi_TR/136900_136999/136942/19.00.00_60/tr_136942v190000p.pdf (accessed on 23 July 2026).
18. 3rd. Generation Partnership Project (3GPP). *TR 38.901: Study on Channel Model for Frequencies from 0.5 to 100 GHz*; 3GPP: Sophia Antipolis, France, 2016. Available online: https://www.3gpp.org/DynaReport/38.901.htm (accessed on 31 July 2026).
19. International Telecommunication Union Radiocommunication Sector (ITU-R). *Recommendation ITU-R P.2109-2: Prediction of Building Entry Loss*; ITU: Geneva, Switzerland, 2023. Available online: https://www.itu.int/rec/R-REC-P.2109-2-202308-I/en (accessed on 29 July 2026).
20. Maral, G.; Bousquet, M.; Sun, Z. *Satellite Communications Systems: Systems, Techniques and Technology*, 6th ed.; Wiley: Hoboken, NJ, USA, 2020; ISBN 978-1-119-38208-9. [CrossRef]
21. International Telecommunication Union Radiocommunication Sector (ITU-R). *Recommendation ITU-R S.1528-0: Satellite Antenna Radiation Patterns for Non-Geostationary Orbit Satellite Antennas Operating in the Fixed-Satellite Service Below 30 GHz*; ITU: Geneva, Switzerland, 2001. Available online: https://www.itu.int/rec/R-REC-S.1528-0-200106-I/en (accessed on 25 July 2026).
22. International Telecommunication Union (ITU). *Radio Regulations, Edition of 2024*; Articles 21 and 22; ITU: Geneva, Switzerland, 2024.
23. Pérez-Neira, A.I.; Vázquez, M.A.; Shankar, M.R.B.; Maleki, S.; Chatzinotas, S. Signal Processing for High-Throughput Satellites: Challenges in New Interference-Limited Scenarios. *IEEE Signal Process. Mag.* **2019**, *36*, 112–131. [CrossRef]
24. Höyhtyä, M.; Mämmelä, A.; Chen, X.; Hulkkonen, A.; Janhunen, J.; Dunat, J.-C.; Gardey, J. Database-Assisted Spectrum Sharing in Satellite Communications: A Survey. *IEEE Access* **2017**, *5*, 25322–25341. [CrossRef]

Disclaimer/Publisher's Note: The statements, opinions and data contained in all publications are solely those of the individual author(s) and contributor(s) and not of MDPI and/or the editor(s). MDPI and/or the editor(s) disclaim responsibility for any injury to people or property resulting from any ideas, methods, instructions or products referred to in the content.